AD-A164 441 GEOSTATIONARY SATELLITE ANALYSES OF PRECIPITATION AND CLOUD PARAMETERS(U) NAVAL POSTGRADUATE SCHOOL MONTEREY CA L A SPRAY DEC 85 1/2

UNCLASSIFIED F/G 4/2 NL

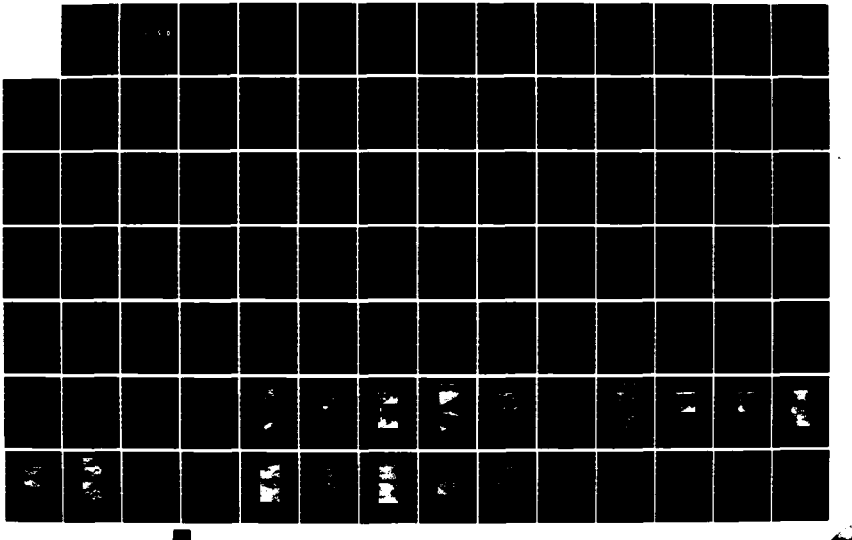

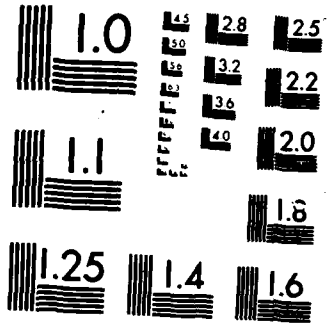

MICROCOPY RESOLUTION TEST CHART
NATIONAL BUREAU OF STANDARDS-1963-A

AD-A164 441

(2)

NAVAL POSTGRADUATE SCHOOL

Monterey, California

DTIC
ELECTE
FEB 2 0 1986
S D
D

THESIS

GEOSTATIONARY SATELLITE ANALYSES
OF PRECIPITATION AND CLOUD PARAMETERS

by

Laura Ann Spray

December 1985

Thesis Advisor: C. H. Wash

Approved for public release; distribution unlimited.

DTIC FILE COPY

UNCLASSIFIED

SECURITY CLASSIFICATION OF THIS PAGE

ADA 164411

REPORT DOCUMENTATION PAGE

1a. REPORT SECURITY CLASSIFICATION UNCLASSIFIED	1b. RESTRICTIVE MARKINGS
2a. SECURITY CLASSIFICATION AUTHORITY	3 DISTRIBUTION / AVAILABILITY OF REPORT Approved for public release;
2b. DECLASSIFICATION / DOWNGRADING SCHEDULE	distribution unlimited.
4 PERFORMING ORGANIZATION REPORT NUMBER(S)	5. MONITORING ORGANIZATION REPORT NUMBER(S)
6a. NAME OF PERFORMING ORGANIZATION Naval Postgraduate School 6b. OFFICE SYMBOL (If applicable) 63	7a. NAME OF MONITORING ORGANIZATION Naval Postgraduate School
6c. ADDRESS (City, State, and ZIP Code) Monterey, California 93943-5100	7b. ADDRESS (City, State, and ZIP Code) Monterey, California 93943-5100
8a. NAME OF FUNDING / SPONSORING ORGANIZATION 8b. OFFICE SYMBOL (If applicable)	9. PROCUREMENT INSTRUMENT IDENTIFICATION NUMBER
8c. ADDRESS (City, State, and ZIP Code)	10. SOURCE OF FUNDING NUMBERS PROGRAM ELEMENT NO. / PROJECT NO / TASK NO / WORK UNIT ACCESSION NO

11 TITLE (Include Security Classification)

GEOSTATIONARY SATELLITE ANALYSES OF PRECIPITATION AND CLOUD PARAMETERS

12 PERSONAL AUTHOR(S)
Spray, Laura A.

13a TYPE OF REPORT	13b TIME COVERED	14 DATE OF REPORT (Year, Month, Day)	15 PAGE COUNT
Master's Thesis	FROM _____ TO _____	1985 December	101

16 SUPPLEMENTARY NOTATION

17 COSATI CODES			18. SUBJECT TERMS (Continue on reverse if necessary and identify by block number)
FIELD	GROUP	SUB-GROUP	Geostationary Satellite Analyses Visible Infrared Thresholds

19 ABSTRACT (Continue on reverse if necessary and identify by block number)

Satellite and surface data are utilized to analyze mesoscale and subsynoptic cloud and precipitation patterns. Digital GOES (Geostationary Operational Environmental Satellite) visible and infrared data are used to produce high resolution (4 n mi) satellite analyses of cloud amount, cloud type, cloud-top temperature and height, and precipitation intensity for an approximate 1600 x 1600 n mi area over the northeastern United States and the western North Atlantic Ocean. Conventional surface observations, the ARS (Automated Radar Summary) chart and manual analysis of the imagery are used to evaluate the satellite-derived analyses for nine cases during the winter and spring 1985.

The majority of cloud amount estimates for clear and overcast sky conditions are analyzed correctly; however, broken and scattered skies are underestimated.

20 DISTRIBUTION / AVAILABILITY OF ABSTRACT	21. ABSTRACT SECURITY CLASSIFICATION
☒ UNCLASSIFIED/UNLIMITED ☐ SAME AS RPT ☐ DTIC USERS	Unclassified
22a NAME OF RESPONSIBLE INDIVIDUAL Carlyle H. Wash	22b TELEPHONE (Include Area Code) (408) 646-2295 22c OFFICE SYMBOL 63Wx

DD FORM 1473, 84 MAR 83 APR edition may be used until exhausted
All other editions are obsolete.

SECURITY CLASSIFICATION OF THIS PAGE
UNCLASSIFIED

#20. - ABSTRACT CONTINUED

The general cloud type patterns are depicted accurately. More success occurs with uniform-textured clouds (i.e. nimbostratus, stratocumulus) and multi-layered clouds than with nonuniform-textured clouds (i.e. cirrus, cumulus). The majority of cloud-top temperature/height analyses are representative of the cloud types and patterns. Most precipitation areas are identified correctly; however, the intensity of the precipitation is underestimated.

Approved for public release; distribution unlimited.

Geostationary Satellite Analyses of Precipitation and Cloud Parameters

by

Laura A. Spray
B.S., University of Wisconsin, Madison, 1983

Submitted in partial fulfillment of the requirements for the degree of

MASTER OF SCIENCE IN METEOROLOGY

from the

NAVAL POSTGRADUATE SCHOOL

December 1985

Author: Laura A. Spray
Laura A. Spray

Approved by:
Carlyle H. Wash, Thesis Advisor

Phil A. Durkee, Second Reader

Robert J. Renard, Chairman,
Department of Meteorology

John N. Dyer, Dean of Science and
Engineering

By
Distribution/
Availability Codes
Dist | Avail and/or Special
A-1

ABSTRACT

Satellite and surface data are utilized to analyze mesoscale and subsynoptic cloud and precipitation patterns. Digital GOES (Geostationary Operational Environmental Satellite) visible and infrared data are used to produce high resolution (4 n mi) satellite analyses of cloud amount, cloud type, cloud-top temperature and height, and precipitation intensity for an approximate 1600 x 1600 n mi area over the northeastern United States and the western North Atlantic Ocean. Conventional surface observations, the ARS (Automated Radar Summary) chart and manual analysis of the imagery are used to evaluate the satellite-derived analyses for nine cases during the winter and spring 1985.

The majority of cloud amount estimates for clear and overcast sky conditions are analyzed correctly; however, broken and scattered skies are underestimated. The general cloud type patterns are depicted accurately. More success occurs with uniform-textured clouds (i.e. nimbostratus, stratocumulus) and multi-layered clouds than with nonuniform-textured clouds (i.e. cirrus, cumulus). The majority of cloud-top temperature/height analyses are representative of the cloud types and patterns. Most precipitation areas are identified correctly; however, the intensity of the precipitation is underestimated.

TABLE OF CONTENTS

LIST OF TABLES

LIST OF FIGURES

ACKNOWLEDGEMENT

I would like to express my gratitude to several people who contributed their valuable time and expertise towards this research effort. I would like to thank Dr. Chuck H. Wash, my thesis advisor, for his knowledge, guidance and support and Dr. Phil A. Durkee for his helpful suggestions and for acting as a second reader. Many thanks to Lang Chou and Mike Gunning for all their time, patience and knowledge of meteorology and computer programming. I would also like to acknowledge Mrs. Linda Rodriguez of NEPRF for assisting with the satellite data collection.

I. INTRODUCTION

Satellite imagery and conventional surface data are primary data sources describing mesoscale weather features. Each provides a different perspective on mesoscale and subsynoptic processes. Continuous satellite imagery provides high resolution analyses of cloud systems from above while the coarser resolution conventional surface data describes the current ground-observed weather conditions. A basic problem is the integration of conventional surface data with satellite data. This problem is addressed here as both surface and satellite cloud data are utilized to analyze mesoscale and subsynoptic cloud and precipitation patterns.

A cloud and precipitation analysis was developed (Wash et al., 1985) that uses digital GOES (Geostationary Operational Environmental Satellite) visible and infrared data to provide high resolution (4 n mi) satellite analyses. This analysis model uses Harris and Barrett's (1978) method to estimate cloud amount; a variation of Liljas' (1982) cloud-typing and precipitation intensity scheme; and Reynolds and Vonder Harr's (1977) bispectral method to derive cloud-top temperature.

The first objective of this thesis is to attempt to generalize the Naval Postgraduate School (NPS) model (Wash et al., 1985) by modifying the infrared thresholds used in the algorithm to account for monthly variations in surface and cloud-top temperature. The second objective is to monitor and evaluate the NPS-model's performance, using the newly-developed

thresholds, with data from the winter and spring seasons. A detailed evaluation of several summer cases was conducted by Wash et al. (1985).

Chapter II presents recent cloud research involving digital satellite data. Chapter III describes the current NPS cloud and precipitation model and Chapter IV discusses how the algorithm used in the model was generalized for use in any season. The subjective and objective plan used in evaluating the model's performance is described in Chapter V, with the results presented in Chapters VI, VII and VIII. Conclusions and recommendations for further investigation are found in Chapter IX.

II. RECENT CLOUD RESEARCH USING DIGITAL SATELLITE DATA

During the past decade the determination of various cloud parameters using digital satellite data has been a vigorous area of research. Algorithms using bispectral thresholds, spatial coherence and radiative transfer computations have been developed to examine various cloud parameters such as cloud amount, cloud brightness and cloud-top temperature.

Shenk, Holub and Neff (1975) developed a cloud type identification scheme for tropical ocean areas using Nimbus-3 MRIR (Medium Resolution Infrared Radiometer) multispectral data from four spectral regions (.2-4 μm, 6.4-6.9 μm, 10-11 μm, 20-23 μm). Infrared thresholds used in making cloud type decisions were based on a radiative transfer model developed by Kunde (1967), which requires input of temperature/moisture soundings and assumed maximum cloud-top heights for low (750 mb) and middle (450 mb) clouds in tropical ocean regions. It was assumed that cirrus and cumulonimbus cloud tops only existed above 300 and 250 mb, respectively. The visible reflectance thresholds were based on the past experience of the authors; low visible thresholds for clear ocean regions were based on an earlier scheme of Shenk and Salomonson (1972). The results of twenty case studies were successful; the derived cloud-type identification maps compared well to high resolution cloud photography.

Minnis and Harrison (1984) examined the effects of extensive cloudiness over a large area using 8 km resolution GOES-E visible (.55-.75μm) and infrared (10.5-12.5 μm) data. They developed a

hybrid bispectral threshold method to extract the following radiative parameters: effective cloud-top temperatures and clear-sky temperature, cloud cover at three altitudes; cloud and clear-sky visible reflectance properties. Cloud amounts and cloud-top temperatures are estimated for all three cloud levels (as well as total cloud cover) using a measured clear-sky temperature and infrared histogram containing infrared threshold counts corresponding to each level's cloud-base temperature determined by a lapse rate. The mean cloud brightness is computed using the infrared threshold-derived value of cloud amount, with the clear-sky brightness determined from minimum reflectance models and the measured average visible count. Surface-based cloud observations and photo analyses were used for evaluation purposes. Their results were reasonable; satellite-derived cloud amount estimates were $\pm.05$ less than both ground observations and photo analyses. Agreement in estimating cloud cover was best at lower and higher cloud amounts and worst with cloud amounts near 50%.

Coakley and Baldwin (1984) developed the spatial coherence approach for retrieving cloud cover for simple-layered systems using 8 km resolution NOAA-7 AVHRR (Advanced Very High Resolution Radiometer) GAC (Global Area Coverage) data. Their algorithm was designed to obtain cloud properties relating to climate studies rather than process imagery data. The spatial coherence method provides the fractional cloud amount and mean cloud-covered radiance. The plot of mean radiance versus standard deviation, which are calculated for each 2 x 2 array of GAC infrared data, has the shape of an arch. Uniform emission from all four pixels

is expected for either a cloud-free or completely cloud-covered oceanic region. Partially cloud-covered pixel arrays rarely exhibit uniform emission. Therefore, the mean cloud-free and cloud-covered radiance values can be identified as the feet of the arch (low standard deviations) and the partially cloud-covered arrays make up the body of the arch. Coakley and Baldwin use only the 11 μm channel to calculate the means and standard deviations of the radiances to determine cloud cover but calculate the visible means and standard deviations to check the infrared values. The least reflective visible values should coincide with the warmest infrared values. The spatial coherence method is limited to ocean regions since land as a background is too variable. It is also restricted to simple-layered cloud systems and assumes that clouds are optically thick at the wavelength of observation. Therefore, the spatial coherence method is inapplicable to baroclinic zones (too complex), ITCZ (non-layered structure) and cirrus clouds (too transparent). For a three-day period over a 250 km area, Coakley and Baldwin found the typical uncertainty in estimating cloud cover to be 14%.

Platt (1983) examined the bispectral method for determining cloud parameters as well as separating broken and semitransparent cloud types using GMS-1 visible (.5-.7 μm) and infrared (10-12μm) data. Bispectral data are used to estimate cloud cover and optical depth, and to identify different cloud types. Unbroken clouds with variable optical depths (i.e. cirrus) are distinguished from broken clouds with uniform optical depths (i.e. stratocumulus) by comparing the shapes of bispectral curves

(infrared brightness temperature vs. visible albedo). Platt discovered the following relationships: albedo increases rapidly with decreasing infrared brightness temperature when the optical depth approaches unity; the albedo and infrared brightness temperature increase with cloud amount. Platt concluded that the best three-dimensional cloud representation would be a combination of the bispectral and spatial coherence methods.

Tsonis (1984) developed an analysis scheme which identifies general sky and surface conditions. His classification groups are clear skies/snow cover, clear skies/no snow cover and high/low broken clouds and overcast. He uses GOES visible (.7 μm) and infrared (11.5 μm) data with spatial resolutions of 4 x 4 km and 8 x 8 km, respectively. The infrared raw counts are converted to temperatures and the visible raw counts are normalized to account for sun angle. The two primary procedures in his separation method are segmentation and classification. Tsonis segments the image into spatially continuous clusters and classifies these groups based upon spectral thresholds and spatial textural features. He defined the cloud/no cloud threshold range to be between 24 and 27 raw GOES sensor counts (corresponding to albedos of 0.12 - 0.19) depending upon the surface characteristics. Tsonis verified his classification results with ground synoptic reports. His agreement percentage with ground truth data was 72%. This percentage increased to approximately 87% when all clouds were considered as one category.

The algorithm used in the NPS model is most closely related to the method of Tsonis (1984). Both use spectral thresholds and

spatial textual characteristics of the visual data to determine various cloud parameters and the satellite-derived analyses are verified with ground synoptic observations. Like Shenk et al. (1975) and Platt (1983) a cloud type identification scheme based on infrared and visible thresholds is used in the NPS model. Coakley and Baldwin's (1984) spatial coherence scheme and Minnis and Harrison's (1984) hybrid bispectral threshold method were designed for climatological studies; the NPS model, which is described in the following chapter, was developed to analyze mesoscale real-time imagery.

III. THE GEOSTATIONARY SATELLITE CLOUD AND PRECIPITATION ANALYSIS MODEL

A general description of the automated NPS cloud and precipitation model is presented. (For further information, refer to the technical report of Wash *et al.* (1985) or Moren (1984).)

The NPS model uses operational digital satellite data from the visual and infrared channels from the GOES Visual-Infrared Spin Scanner Radiometer (VISSR). The NPS model creates real-time analyses of cloud amount, cloud type, cloud-top temperature, cloud-top height and precipitation intensity. The model processes the satellite data, performs statistical calculations, and produces cloud and precipitation analyses.

Visual raw data counts are converted to albedos using a normalization scheme that corrects for sun angle and anisotropy (Muench and Keegan, 1979). Infrared data counts are converted to temperatures using the GOES sensor conversion table (Corbell *et al.*, 1978). For each 2 x 2 grid of visual data, an average brightness and standard deviation is computed. The average visible brightness and corresponding infrared temperature are used in the final cloud and precipitation analyses.

The hybrid bispectral threshold method of Reynolds and Vonder Haar (1977) is used to estimate cloud amount. Cloud amount is determined by comparing the visual albedos with a pre-established cloud/no cloud threshold of 0.15. If the albedo is greater than or equal to the 0.15 threshold, the pixel is considered cloudy. The cloud/no cloud threshold was lowered from 0.17, the value used in the summer evaluation (Wash *et al.*,

1985), to 0.15 so that more small cumulus could be identified. The 0.15 threshold compares well with the 0.13 threshold used by Keegan and Niedzielski (1981), who looked at 1977-78 autumn/spring/summer data over the northeastern United States, and the 0.12 - 0.19 albedo range used by Tsonis (1984). An average cloud amount for each 2 x 2 grid is calculated (Harris and Barrett, 1978; Fye, 1978). A larger analysis array would provide a more complete range of cloud amounts but take longer to execute.

Cloud type is determined through a series of threshold tests that use both infrared temperatures and visual albedos (Liljas, 1982). The infrared thresholds have been modified to compensate for the monthly variation in the infrared temperatures. These modifications are discussed in the following chapter. In addition, a texture test that computes the standard deviation of each 2 x 2 grid of visual data is performed to differentiate between cumuliform and stratiform clouds which often have similar visible and infrared (11 μm) radiative properties (Liljas, 1984).

The precipitation estimation method, a modified version of Liljas' (1982) threshold technique adopted from the results of Muench and Keegan (1979), applies the cloud type information to the precipitation areas. The precipitation module is activated if the cloud-type decision is nimbostratus or cumulonimbus. The magnitude of intensity is dependent upon the infrared and visual values; the colder infrared temperatures and brighter visual albedos produce heavier intensities (Liljas, 1984). The infrared precipitation/no precipitation threshold, which varies from 247.5

K to 254 K, compares well with the 246 K to 253 K temperature range of Paul (1983).

Cloud-top temperatures are estimated using a bispectral approach (Reynolds and Vonder Haar, 1977) that provides a better analysis of cloud-top temperatures for partially-filled fields of view and cirrus layers since the amount of surface radiance is estimated. Cloud-top temperatures are derived from the computed radiance, which takes into account surface and cloud radiance, emissivity and cloud amount. Finally, the cloud-top temperatures are equated to the pressure level heights from the Fleet Numerical Oceanography Center (FNOC) grid-point temperature profiles.

The following chapter describes how the model is made applicable for use in various seasons. The infrared thresholds used in the cloud-typing scheme were modified to compensate for the monthly variation in the infrared temperatures.

IV. GENERALIZATION OF ALGORITHM

The more difficult objective of this research effort is to generalize the algorithm used in the NPS model so that it can be applied for any month. It was observed from the analysis of the winter and spring cases, discussed in the following chapters, that the cloud infrared temperatures become progressively warmer from January to May. The infrared thresholds specifying various cloud groups need to be modified to compensate for this warming. Manual nephanalysis and conventional surface data were used to tune the initial winter and spring case studies to arrive at a set of infrared thresholds for each case. Independent cases are used to test the new infrared thresholds.

The visible thresholds as well as the infrared thresholds used in this investigation (Figs. 1-5) differ from the earlier summer values (Fig. 6). The following modifications were made to the visible thresholds: The cloud/no cloud threshold was lowered from 0.17 to 0.15; the visible threshold differentiating cirrus from nimbostratus/multi-layered or altostratus/cumulus congestus was lowered from 0.55 to 0.32; the upper visible threshold defining stratus was raised from 0.55 to 1.0 while the lower visible threshold defining stratocumulus was lowered from 0.55 to 0.15 (stratocumulus and stratus are now only distinguished in the infrared spectrum); nimbostratus/multi-layered and cumulonimbus are now differentiated by a visible threshold 0.88 (> 0.88 results in a cumulonimbus classification) but can have similar infrared characteristics. These modifications resulted from the

investigation of the analysis errors that occurred in the summer cases discussed in Wash et al. (1985). The visible thresholds are not altered throughout this study.

The infrared thresholds defining low-level cloud types stratocumulus, cumulus and stratus exhibit the most variation from month to month. Liljas (1984) found that stratus cloud-top temperatures may vary up to twelve degrees during the summer. Maturi and Holmes (1985), who developed monthly infrared imagery enhancement curves for sea fog, used enhancement curves that varied from 276 K - 281 K in April to 287.5 K - 293 K in August. A threshold scheme, which utilizes real-time satellite data, takes into account daily temperature fluctuations; an infrared enhancement method, which uses pre-determined enhancement curves, may not identify small temperature pertubations.

In the 17 Jan study, the infrared temperatures which classify stratocumulus are 256-266 K (Fig. 1). In the 28 Mar case, stratocumulus is classified between 286-265 K (Fig. 3) which is at least nine degrees warmer than the stratocumulus in the 17 Jan case. This warming trend is evident in the scattergram (Fig. 7) in which the visible and infrared raw data counts (lower infrared count for warmer temperature) corresponding to surface reports of stratocumulus are plotted for each case. The stratocumulus of the 28 Mar case (represented by the symbol X) is warmer than the stratocumulus of the 17 Jan case (represented by the symbol O). A similar temperature variation occurs with stratus and cumulus clouds. The stratus and cumulus clouds appear to be at least ten degrees warmer in May than January; this is illustrated in Fig. 8.

A dramatic increase in infrared temperatures from January to May does not occur with middle-to-upper level clouds. The raw infrared counts of the multi-layered reports for each case exhibit a random pattern (Fig. 9) rather than a January to May warming trend. Therefore, the 247.5 K temperature threshold defining nimbostratus/multi-layered and cumulonimbus in the 17 JAN case is only raised by 6.5 degrees to 254 K for the subsequent cases. The small threshold adjustment also applies for cirrus and altostratus/cumulus congestus.

The significant temperature difference between months found with low-level clouds is due to the increase in surface temperatures from January to May. This surface and low cloud warming trend is illustrated in the three-dimensional cluster diagrams (Figs. 10-12). The number in the darkened regions represents the average frequency of occurrence (higher frequency in the darker regions) of each infrared and visible (scaled to the infrared data by multiplying by four) count combination that occurs within the image. For example, in the January cluster diagram (Fig. 10), there are approximately 157 occurrences of an infrared count of 75 (293 K) and visible count of 60 (15 x 4; albedo of 0.02). The blank horizontal lines represent raw counts that are missing in the infrared imagery. The cluster diagrams separate the satellite digital data into clusters of similar visible and infrared raw counts. Each cluster can be identified in the images. For example, the cluster in the middle of Fig. 10 (17 Jan) can be identified as stratocumulus clouds since the stratocumulus observed in the GOES imagery (Figs. 13 and 14)

possess these visible and infrared raw count values. The cluster diagrams indicate that upper-level clouds do not have much monthly temperature variation. A similar clustering scheme used by Hawkins (1980) separates only infrared imagery into different radiative regions in which attributes are evaluated for the various clusters.

The performance of the NPS model, using the new infrared thresholds, was monitored and evaluated for several 1985 winter and spring case studies. The evaluation plan and results are described in the following chapters.

V. EVALUATION PLAN

The eastern United States served as the evaluation region for this investigation. This geographical location was selected due to abundant verification data, variety of meteorological phenomena (including coastal, land and cloud features) and the ability for direct comparison to the summer results for the same area (Wash et al., 1985).

GOES visible and infrared data, which are collected at the Naval Environmental Prediction Research Facility (NEPRF) in Monterey, California, are modified to provide a center point at 35^{o} N 80^{o}W for a 512 x 512 array with 2 x 2 n mi visual (2 x 4 n mi infrared) resolution. The 512 x 512 array is divided into sixteen 64 x 64 grids. For each of the sixteen center points of the grids, a 1200 GMT surface and upper-level temperature profile is obtained from the Fleet Numerical Oceanography Center (FNOC). The final output cloud and precipitation fields are 256 x 256 grid arrays which approximately covers a 1024 x 1024 n mi area.

The verification data network over the eastern United States consists of National Meteorological Center (NMC) facsimile charts, FNOC synoptic land, ship and surface airway reports, and manual nephanalysis.

Nine winter and spring cases were chosen to monitor and evaluate the performance of the NPS cloud and precipitation model using the new infrared thresholds. Five cases were used to create the new winter and spring thresholds used in the algorithm and four were used as independent test cases. Data collection

consisted of capturing coincident infrared and visible data as well as the verification data for 1800 GMT 17 Jan, 20 Mar, 28 Mar, 11 Apr, 13 May (initial cases) and 20 Feb, 27 Mar, 16 Apr, 15 May, 1985 (independent test cases). A subjective and statistical evaluation was performed on each case in which the NPS model output was compared to the conventional data.

Direct comparison between ground-observed sky conditions and satellite digital data is a difficult task. Tsonis (1984) cites the following difficulties:

> An observer reports the sky conditions for an area that is obviously larger than the area represented by point...Therefore, comparison between the satellite classification (corresponding to a point that coincides with the geographical location of the synoptic station) and the station's report may be quite inadequate...Furthermore, any classification by an observer, as "higher" or "lower" clouds is less objective than that by a satellite...The following reasons are given:the observer...looks at a much larger area, seeing the clouds in that area at different angles. Individual reactions, as well as human error, may contribute to the classification. The satellite, on the other hand, will indicate higher or lower clouds by its infrared count at each point;such a procedure is very objective. Another fact that may give rise to problems is that the observer looks at the clouds from below, whereas the satellite looks from above.

These ground-satellite perspective difficulties encountered in this investigation will be discussed further in the following chapters.

VI. SUBJECTIVE EVALUATION RESULTS

The subjective evaluation results of the model's performance in the 17 Jan case are presented in full along with an overview of its performance on the other days studied. In general, the model produced accurate cloud amount, cloud-type, cloud-top temperature/height and precipitation intensity maps in each case.

In this January case, the primary synoptic features are a warm front, which extends from a 1000 mb low pressure center located at 37^{o}N 75^{o}W, and a cold front that extends from Florida to the Gulf of Mexico. Extensive cloudiness and precipitation are associated with this frontal system as evident in the GOES visible and infrared imagery (Figs. 13 and 14). A secondary feature is an occluded front, extending into eastern Pennsylvania associated with a 996 mb low pressure center, which produced snow and snow showers throughout the region.

Each cloud amount category is depicted by a particular color. In this case, the NPS model depicts the extensive overcast (blue) covering the majority of the region as well as the broad clear zone (gray) south of the front over the southern tip of Florida and adjacent waters (Fig. 15). Broken/overcast (dark green), broken (light green) and scattered (red) sky conditions are underestimated in the southeast quadrant.

The estimation of cloud amount is directly related to the size of the array used in making the cloud amount decision, which is determined by the number of pixels with albedos greater than the 0.15 cloud/no cloud threshold. A 2 x 2 matrix (approximately

4 n mi) of visible data used in the model allows only four fractional cloud amount estimates: 25%, 50%, 75%, 100%. Increasing the number of albedos (larger field of view) used in making the cloud amount decision would yield a better range of fractional cloud amounts which would lead to more estimates of broken and scattered skies.

The eight cloud type classifications of the 17 Jan case, which are represented by a different color, are presented in Fig. 16. The extensive stratocumulus field (light green) associated with the cold air to the rear of the baroclinic zone is correctly depicted by the model. The cirrus (red) and altostratus (orange) located in the northern quadrant of the image are also classified correctly. The model's analysis of the large stratus (yellow) and cumulus field (dark green) located in the southwest quadrant is verified by manual imagery analysis. The NPS model also indicates correctly the line of cumulonimbus (dark blue) over northern Florida.

The model produced a different cloud-type analysis than the ground observations in the eastern quadrant due to the difference in perspective between the ground and the satellite. The model cloud-typing decision for this area is nimbostratus/multiple layers (blue) while many surface stations report stratocumulus. The infrared temperatures range from 251-235 K and the albedo values are all greater than 0.55. The satellite senses cold infrared temperatures, indicating middle/high clouds, while the surface observer views only the low cloud layer. The ground observer can not distinguish the upper cloud layers.

The NPS cloud-top temperature analysis (Fig. 17) depicts a range of temperatures (220-290 K) which corresponds to the wide variety of cloud layers and types found in this 17 Jan case. Each of the nine colors corresponds to a 10 K cloud-top temperature interval which ranges from 210-219 K (dark blue); to 290-300 K (gray). Over northern Florida the analyzed cloud-top temperatures are 220 K (blue) and 230 K (light blue), which verifies with the surface reports of cumulonimbus and the 1835 GMT Automated Radar Summary (ARS) chart (Fig. 18).

The cloud-top height analysis (Fig. 19) follows the temperature analysis since cloud-top height is a function of cloud-top temperature. Each of the nine colors corresponds to a 100 mb cloud-top height interval which ranges from 100-199 mb (dark blue) to 900-999 mb (dark red).

The NPS model defines two precipitation areas: northern Florida and along the eastern seaboard. Three colors are used to describe precipitation intensity: red, green and blue denote light, moderate and heavy intensity, respectively. The model distinguishes the squall line over Florida with estimates of all three degrees of intensities (Fig. 20). This is verified by the 1835 GMT ARS chart (Fig. 18) where light rain (red) to heavy thunderstorms (blue) are detected by the radar. Light (red) and moderate (green) precipitation is associated with the frontal zone. This is also verified by the 1835 GMT ARS chart but only two coastal surface stations (indicated by the arrows) report precipitation in this area (Fig. 21). The model overestimates the frontal precipitation. Overall, the NPS cloud and precipitation model performed well in the 17 Jan case.

The spring cases (20 Mar, 28 Mar, 11 Apr and 13 May) were also evaluated subjectively. The highlights of the evaluation are presented for each cloud parameter: cloud amount, cloud type, cloud-top temperature/height and precipitation intensity.

Cloud amount estimates are generally accurate for overcast and clear skies. The broken/overcast, broken and scattered situations tend to be underestimated since only four visible albedos are used in determining cloud amount.

Some small cumulus elements are not identified as clouds since their albedos are below the 0.15 visual cloud/no cloud threshold. The small cloud elements do not fill the sensor's field of view; therefore, surface reflectivity influences the cloud/no cloud decision and cumulus is classified as clear skies. This is evident in the 20 Mar case (Fig. 22) where some small cumulus in Florida, as seen in the GOES visible and infrared imagery (Figs. 23 and 24), are not identified.

Cloud amount is overestimated when snow cover is mistaken for cloud cover (Minnis and Harrison, 1984). An example of this situation is found over Ontario north of Lake Erie in the 11 Apr case. This area is classified as cloudy (Fig. 25) due to bright albedos (> 0.15) and cold infrared temperatures (270 K) but is really clear and snow-covered as seen in the GOES visible and infrared imagery (Figs. 26 and 27); this is verified by the snow cover map in Fig. 28. The AFGWC Automated Cloud Analysis Model does not calculate cloud amount whenever snow is present at a grid point; clouds can not be discerned from snow (Fye, 1978). Generally, the cloud/no cloud decision is made correctly in the

spring cases but the scattered and broken classifications are underestimated.

In the spring studies the cloud type classifications that are the most successful are large areas of uniform-textured clouds such as nimbostratus and stratocumulus. For example, in the 28 Mar case (Fig. 29) the model identifies the multiple-layered clouds (blue) of the baroclinic zone, and the stratocumulus (light green) and cumulus (dark green) to the rear of the front, as evident in the GOES visible and infrared imagery (Figs. 30 and 31).

Common cloud-typing errors are: (1) clear skies with snow-covered ground classified as stratocumulus and cumulus clouds; (2) semitransparent cirrus classified as clear skies or low cloud; (3) cumulus classified as clear skies.

In the 11 Apr case the NPS model specifies the clear snow-covered areas in the northwest quadrant as stratocumulus (light green) (Fig. 32) since both the visible threshold (0.15) and the infrared threshold (291 K) are exceeded.

Another common misclassification occurs with cirrus-type clouds. Semitransparent cirrus, which is located in the Carolinas and Tennessee, is identified as clear skies in the 11 Apr case (Fig. 32). The surface radiation reaching the sensor results in extraordinarily warm infrared temperatures which causes the misclassification.

Small cumulus are sometimes classified as clear skies. This is illustrated in the 13 May and 28 Mar cases. In the 13 May case the small cumulus in Florida and the southwest quadrant (evident in the GOES visible and infrared imagery, Figs. 33 and

34) are not identified by the model (Fig. 35). In the 28 Mar case the cumulus along the Gulf Coast (evident in the GOES visible and infrared imagery, Figs. 30 and 31) are classified as clear skies by the model (Fig. 29). The small cloud elements do not fill the sensor's field of view which allows surface effects (warm infrared temperatures and dim albedos) to influence the cloud-type identification decision.

The cloud-top temperature/height analyses are fairly accurate in the spring cases. For example, in the 28 Mar case the cloud-top temperature analysis (Fig. 36) depicts the various cloud types associated with the baroclinic zone. Cloud-top temperatures of 220 K (blue) and 210 K (dark blue) represent cirrus-type clouds. Temperatures ranging between 230 K (light blue) and 260 K (light green) indicate multiple-layered clouds and the stratocumulus and cumulus to the rear of the system have cloud-top temperatures between 270 K (yellow) and 280 K (red). The only cloud-top temperature errors occur with semitransparent cirrus and small cumulus for similar reasons as discussed above (i.e. the influence of surface radiation).

Precipitation delineation is reasonable for the majority of spring cases. For example, in the 20 Mar case the large precipitation area identified by the model in the central and southwest quadrant (Fig. 37) is verified by the 1835 GMT ARS chart (Fig. 38) and surface observations. The small precipitation region over Maryland is also correctly identified.

A common precipitation error throughout the investigation is also illustrated in the 20 Mar case. The radar detects

precipitation occurring over western Pennsylvania but the model misses this area since the infrared temperatures are below the precipitation/no precipitation threshold (Fig. 39).

Precipitation intensity is more difficult for the model to estimate and to be evaluated by an investigator. Lovejoy and Austin (1979) conclude that GOES infrared and visible data are good for determining precipitation areas but poor for determining intensities. The biggest error in precipitation intensity is found in the 11 Apr case. The NPS analysis (Fig. 40) indicates light precipitation (red) and the radar detects moderate rain and rain showers off the northeast coast (Fig. 41). Overall, the NPS model can determine precipitation distribution and does a fair job in estimating intensity.

The subjective evaluation results of the model's performance with winter and spring data were described in this chapter. The objective evaluation in the following section presents additional outcomes and supports the preceding conclusions.

VII. OBJECTIVE EVALUATION RESULTS

A statistical evaluation is performed on the cloud type and precipitation parameters for each winter and spring study. The NPS model cloud type and precipitation analyses are compared to conventional surface data.

The verification network used in the evaluation is a combination of 1800 GMT synoptic land, airways and ship data for an area encompassing the satellite image, 25-45° N and 90-70° W. Tsonis (1984) also uses ground synoptic stations to verify his satellite classification scheme.

The surface data processor used, an updated version of the scheme developed by Wyse (1984), only processes cloud type and precipitation information. The surface data analysis methods utilized in the processor are similar to those of Hahn et al. (1984) and are summarized as a flow chart in Fig. 42. The surface observations of sky cover, present weather and low, middle and high cloud type determine the cloud-typing decision. Hahn et al. (1984) and the NPS processor discard the surface report if the sky cover information is missing, if the sky is obscured and there is no precipitation reported, or if there is sky cover reported but the cloud type information is either missing or zero and no report of weather. The NPS version classifies those reports with sky cover less than or equal to three tenths as clear skies. Tsonis (1984) uses this same criterion in his classification scheme. If just the cloud information is missing but present weather exists, the cloud type

is determined by the weather parameter. For example, if the cloud type group is missing but rain is reported, the cloud type decision is nimbostratus.

Synoptic and airways observations are classified into eight categories (Ci, As, St, Sc, Cu, CC, Ns and Cb) corresponding to the World Meteorological Organization (WMO) code (Tables 1-3). The decision process is summarized by Fig. 43. If two or more cloud layers are observed, the report is classified as multiple layers (ML). Two differences between the actual NPS cloud-typing decision process and the Hahn et al. (1984) scheme are that the NPS processor distinguishes between stratus and stratocumulus and cumulus and cumulus congestus.

As seen in Tables 1-3, some cloud type categories are misleading; therefore, special processing decisions are needed. For example, low cloud type 7 (stratus/cumulus of bad weather or both usually below altostratus or nimbostratus) incorporates a middle-level cloud (altostratus, nimbostratus). Therefore, if the cloud cover exceeds five tenths, the classification is multi-layered clouds; if it is less than or equal to five tenths, the resulting cloud classification is stratocumulus. Low cloud type 8 (cumulus and stratocumulus) does not distinguish between the two categories; therefore, these low cloud type reports are ignored. Another example occurs with middle cloud type 7 (altocumulus, etc.). Altocumulus is not distinguished from nimbostratus; therefore, the cloud decision is altostratus/nimbostratus when no precipitation/precipitation is reported.

The precipitation decision is based on the present weather parameter. If the present weather is a WMO code between 50 and 99, precipitation is occurring at the time of the observation.

Each valid surface observation of cloud type is compared to the corresponding NPS model cloud type decision as well as the predominant cloud type of a 7 X 7 matrix which covers an approximately 28 x 28 n mi area. A voting procedure is used on the matrix to determine the cloud type that occurred most frequently in the satellite matrix. A straight percentage is computed for the number of agreements between the surface observation and the satellite information (assuming the surface report to be correct): PERCENTAGE CORRECT = NUMBER OF AGREEMENTS / TOTAL NUMBER. A percentage correct is computed for clear conditions, eight individual cloud type categories (Ci, As, St, Sc, Cu, CC, Ns and Cb) and three cloud group categories (low, middle and high). Surface reports of multi-layered clouds are evaluated in a subjective rather than an objective manner since the NPS cloud-typing routine does not separate multi-layered and nimbostratus clouds.

The multi-layered cloud type category comparison is made between the 7 x 7 satellite matrix and the corresponding surface observation. Surface reports of multiple layers are placed into five separate categories according to the thickness properties of the particular cloud types.

Reports of dense cloud types at two or more levels are classified as multi-layered (i.e. stratocumulus, WMO low cloud type 5 and dense cirrus, WMO high cloud type 2). Ground

observations of semitransparent cloud types at all three levels are categorized as thin clouds. Semitransparent middle and/or lower level cloud types, but dense clouds at upper levels are considered high clouds and thin upper and/or lower layer cloud types, but opaque middle cloud types are designated as middle clouds. Finally, semitransparent cloud types at upper and/or middle levels, but thick at the lower level are classified as low clouds.

Each 7 x 7 matrix corresponding to a surface report of multiple cloud types is also categorized. If two or more cloud types at different levels occur in the matrix, the satellite cloud-typing decision is multi-layered. If the matrix contains mostly zero values (clear conditions), the resulting classification is thin. If the majority of cloud types are cirrus, the decision is high cloud. The matrix is specified as middle cloud if the majority of cloud types are middle cloud (altostratus, nimbostratus) and it is classified as low cloud if the predominant cloud types are low clouds (stratocumulus, stratus, cumulus, cumulus congestus).

Assuming the surface report of multi-layered clouds to be correct, each satellite matrix is compared to the ground truth data. If the surface and satellite do not have the same multi-layered properties, (i.e. surface report is classsified as thin; satellite is specified as multi-layered) the pair is labelled mismatch.

For each case, precipitation occurrence is also evaluated statistically. The surface report of precipitation/no

precipitation is compared to the result of the voting scheme performed on the 7 x 7 matrix in which twenty-four precipitation votes out of forty-nine pixels constitutes precipitation.

Each surface report of precipitation is compared to the NPS model's precipitation decision and a percentage correct is computed: PERCENTAGE CORRECT FOR PRECIPITATION REPORTS = NUMBER OF AGREEMENTS BETWEEN SATELLITE AND SURFACE / TOTAL SURFACE REPORTS OF PRECIPITATION. The same evaluation procedure is used for surface stations where no precipitation is occurring.

The results of the cloud type and precipitation evaluation for the winter and spring cases are found in Tables 4-7. Table 4 contains the statistical results of the specific cloud type categories, the group cloud type statistics are found in Table 5 and the multi-layered results are presented in Table 6. Precipitation results are presented in Table 7.

The most successful cloud type classification is the clear skies category. The percentage correct (one to one correspondence between the NPS model output and surface report) ranges from 71% (11 Apr) to 100% (17 Jan) and a total value of 91% for all cases. In each clear sky case, the 7 x 7 vote produces as good or better results than the single pixel comparison (Tables 4 and 5).

Reasonable results are obtained for the stratiform cloud types, stratocumulus and nimbostratus, for both direct and matrix comparison methods. In most instances these cloud types are specified correct nearly fifty percent of the time. These uniform-textured clouds fill the satellite's field of view and

cover the entire sky; therefore, it is more likely that the satellite sees the same sky conditions as the observer.

Misclassification of nimbostratus in the 17 Jan and 28 Mar cases are due to warm infrared temperatures above the pre-established thresholds causing the cloud decision to be stratocumulus. Ground-observed stratocumulus is either classified as nimbostratus, if the infrared temperatures are too cold, clear/stratus, if the temperatures are too warm, or cumulus, if the texture test produces a high standard deviation (i.e. edge of a stratocumulus cloud located near a synoptic station).

Two exceptions to the good performance by the stratiform class are altostratus and stratus. Both reports of altostratus are classified as stratus by the NPS model due to the satellite sensor's detection of warm infrared temperatures below the pre-established thresholds for altostratus (256 K, 17 Jan; 261 K, 20 Mar). For both cases, the surface report is altocumulus translucidus at a single level (WMO middle cloud type 3, Table 2). Due to the transparent nature of this type of middle cloud, surface radiation reaches the sensor, causing the misclassification.

There are also model-observation disagreements with stratus. In all five cases, this classification error can be attributed to infrared temperatures that are too cold; the temperatures exceed the thresholds and are specified as altostratus or nimbostratus. This error is an example of the limitations of objectively evaluating cloud detection. A difference in perspective between the ground observer (looks up) and the satellite (looks down)

causes this stratus misclassification. The ground observer is unable to detect the upper cloud layers that the satellite senses due to the opaque nature of the lowest cloud layer (Bunting and Hardy, 1984; Tsonis, 1984); therefore, the surface report of stratus (lowest layer) and the NPS model cloud-typing decision of nimbostratus/altostratus do not agree.

Misclassifications also occur with nonuniform or rough-textured clouds such as cumulus, cumulus congestus and cumulonimbus. The incorrect NPS model cloud type classifications are due to either low albedo values, warm infrared temperatures or error in texture determination.

Many of the surface reports of cumulus have visible albedo values less than the visible cloud/no cloud threshold (0.15). The small cumulus do not fill the satellite's field of view resulting in a classification of clear skies. The sensor is unable to resolve the individual cumulus clouds that the observer is able to see. Direct comparison between the surface observation and corresponding satellite pixel produced better results than the 7 x 7 matrix voting procedure (Table 4). When the field of view is smaller, the small cumulus elements are more likely to be resolved. This illustrates another difficulty in relating the ground-based observation to data collected from satellites.

Many cumulus, cumulus congestus and both cumulonimbus reports also have infrared temperatures that are warmer than the pre-established thresholds due to the influence of surface radiation. Therefore, cumulus is classified as clear skies and cumulus

congestus and cumulonimbus are classified as either cumulus or clear skies. The majority of surface observations of cumulus congestus, analyzed as cumulus by the model, are ship reports. These ship reports are probably classified correctly as cumulus since cumulus congestus is a cloud type that is more likely to exist over land (more surface heating) than over water.

Some surface reports of cumulus are classified as stratocumulus or stratus due to low standard deviation values signifying smooth textures. Changing the standard deviation criteria did not solve this problem since other correctly-classified stratocumulus and stratus clouds were then incorrectly categorized as cumulus.

The disagreements between the NPS model output and the surface observations of cirrus are also due to extremely warm infrared temperatures. Many of the ground-observed cirrus-type clouds are cirrus fibratus (WMO high cloud 1) or cirrostratus not progressively invading the sky (WMO high cloud 8), which are nearly transparent (Table 3). Optically thin cirrus are semitransparent to the upward directed radiation which allows the underlying area and clouds to contribute to the cloud-typing decision. All three correct cirrus classifications are of the type cirrostratus covering the entire sky (WMO high cloud 7) which fills the sensor's field of view; the cold infrared temperatures associated with this type of cirrus are well below the thresholds.

An improvement in the cloud-typing statistics occurs when similar types of clouds are merged together such as the low clouds, cumulus, stratocumulus, stratus and cumulus congestus and

middle cloud type altostratus and nimbostratus. For example, in the 20 Mar case there are only two correct classifications in the direct surface-satellite comparison and 7 x 7 matrix (Table 4). Five out of twelve (42%) correct classifications are made when the low clouds are considered as one group (Table 5). The coarse resolution of the satellite data relative to the surface observer and the difference in viewing geometry limits the number of categories that can be distinguished by the NPS satellite algorithm (Bunting and Hardy, 1984).

The majority of surface reports are multi-layered clouds. Since no separate distinction for multiple cloud layers is made by the NPS model, a special evaluation procedure is utilized. Most of the NPS model decisions are in agreement with the surface categorizations. For example, in the 13 May case, of the twenty-one surface reports of multi-layered clouds, there are nine belonging to the THIN category, four of type CL, three of type ML, one of type CM and CH and only three mismatches (Table 7).

There are only two causes of mismatches between the satellite and conventional data: the edges of multiple cloud systems are located near synoptic stations which results in satellite decisions of clear skies or low clouds; and reports of low and high clouds are classified as middle cloud since the sensor detects a large dense cloud mass and is unable to distinguish between the different layers. The NPS model does a fair job portraying the multi-layered cloud systems.

The objective precipitation statistics are presented in Table 7. The NPS model is able to delineate most precipitation areas

since the majority of surface observations of precipitation are identified by the model. The total percentage correct value for all reports of precipitation is 49% with a range of values from 41% in the 17 Jan case to 100% in the 13 May case.

The discrepancies between the model and ground truth data are caused by infrared temperatures that are warmer than the precipitation/no precipitation threshold. For example, in the 17 Jan case, several observers report precipitation with stratocumulus clouds. The NPS model classifies the stratocumulus correctly, but does not detect the precipitation since the infrared temperatures are warmer than the precipitation/no precipitation threshold of 247.5 K.

Ninety-four percent of all surface reports of no precipitation are in agreement with the satellite analysis (Table 7). The most successful result is 97% in the 13 May case and the least successful percentage correct value (90%) occurs in the 17 Jan study. The satellite-surface disagreement can be attributed to visible and infrared values exceeding their respective thresholds.

In general, the objective evaluation results of cloud type and precipitation identification are encouraging. The following chapter presents the results of the four independent investigations used to test the new thresholds.

VIII. STATISTICAL RESULTS OF THE INDEPENDENT TEST CASES

The statistical results of four independent cases (20 Feb , 27 Mar , 16 Apr and 13 May) used to test the hypothesized thresholds are presented in Tables 8-11. Each new study utilizes the corresponding tuned thresholds of the previous investigations: The 20 Feb case uses 20 Mar thresholds; the 27 Mar case uses the Mar 28 values; the 16 Apr case uses 11 Apr thresholds; and the 15 May case uses the 13 May values.

The results of the objective evaluation of the independent studies are similar to those of the initial cases. The most successful cloud type classification (78% correct for all cases) clear skies category. Percentage correct values range from 63% (20 Feb case) to 100% (16 Apr and 15 May case) with better or at least as good statistics obtained with the 7 x 7 voting scheme (Table 8). The low percentage of the 20 Feb study is related to clear skies over snow-covered ground that the NPS model identifies as low clouds.

The best single cloud type classifications are for stratiform types nimbostratus and stratocumulus. Sixty percent of all nimbostratus reports are classified correctly by the model; percentage correct values range from 25% (15 May case) to 100% (20 Feb case). For stratocumulus the range of values is 29% (27 Mar case) to 50% (16 Apr case) with a total value of 32% for all cases. The statistical outcomes from the 7 x 7 voting procedure are better or as good as the direct pixel- to- station comparison for these uniform-textured clouds. Most of the

disagreement between the model and surface data in the stratocumulus classification is due to the difference in perspective between the ground and satellite. The surface observer views the low cloud stratocumulus while the satellite senses multiple layers. The ground observer can not identify the upper cloud layers.

As in the initial cases, the model has difficulty specifying the other stratiform cloud types stratus and altostratus. Only one of the nine reports of stratus is classified correctly by the model. Most of the stratus, analyzed incorrectly as clear skies, are located on the edges of synoptic stations. The one report of altostratus is analyzed as nimbostratus by the model; the infrared temperatures are colder than the threshold.

Nonuniform-textured cumulus, cirrus, cumulus congestus and cumulonimbus clouds are not easily identified by the model in the test cases. Three out of thirty-one reports of cirrus and two out of eight reports of cumulus are classified correctly. Cumulus congestus and cumulonimbus are never accurately depicted.

The same classification errors for these rough-textured clouds are observed in the test cases as in the initial studies. The cirrus is semi-transparent and the cumulus do not fill the sensor's field of view; surface characteristics influence the sensor's interpretation of the cloud's temperature and albedo causing the analysis error. The five surface reports of cumulonimbus and thirteen reports of cumulus congestus are misclassified as cumulus congestus and cumulus, respectively, when the infrared temperatures are warmer than the predetermined thresholds. Cumulonimbus is analyzed as nimbostratus when the

visible albedos are below the 0.88 visual threshold separating these two cloud types.

The majority of surface reports are of multiple cloud layers and are in agreement with the subjective evaluation of the satellite data. Out of eighty-six multi-layered cloud reports, only five are labelled mismatch--the satellite and surface data are in disagreement (Table 10). The majority of surface reports of multiple cloud layers correspond to a satellite matrix that contains classifications of cloud types at different levels (MULTI).

The precipitation statistics for the independent cases are presented in Table 11. Eighty-three percent of the surface reports of precipitation are recognized by the model. The no-precipitation results are also reasonable. Ninety-three percent of all no-precipitation cases are correct with values ranging from 84% (27 Mar case) to 98% (20 Feb case). As in the initial cases, the only surface-satellite disagreement of precipitation occurrence in the test cases is due to visible and infrared values above or below the precipitation/no precipitation thresholds.

The cloud and precipitation statistical results of the independent test cases resemble the outcomes of the initial investigations. Similar classification successes and failures are noted. The tuned thresholds from the initial studies were successful fairly well for the test cases. Generalizing the NPS model's algorithm by altering the infrared thresholds to account for the observed monthly variation in surface radiation produces

reasonable cloud and precipitation analyses. The successes and limitations of the model as well as recommendations for future research are described in the following chapter.

IX. CONCLUSIONS AND RECOMMENDATIONS

Directly integrating satellite and surface data is a difficult task. Satellite imagery provides important cloud and precipitation information from above while conventional surface data describes weather features from below. This thesis illustrated that using satellite and surface data as complimentary forecasting tools produces better analyses of mesoscale and subsynoptic weather features. The performance of an automated cloud and precipitation model (Wash et al., 1985) that uses GOES visible and infrared data to provide high resolution analyses was evaluated for several 1985 winter and spring days. The infrared thresholds used in the algorithm were modified for each case due to the observed temperature variability from January to May.

The NPS model succeeds in analyzing most overcast and clear skies but underestimates broken and scattered situations. A visible albedo of 0.15 seems to be a representative cloud/ no cloud threshold. Most surface reports of clear skies are in agreement with the model except clear skies over snow-covered ground which is analyzed as low cloud since the visible and infrared thresholds are exceeded.

The cloud type analyses are reasonable. Accuracy increases when all low level clouds or middle level clouds are considered as one cloud type. The majority of large uniform-textured clouds such as nimbostratus and stratocumulus are classified correctly by the model. The 7 x 7 voting scheme is superior to

the direct pixel-station comparison method when evaluating these stratiform clouds. The majority of surface reports of multi-layered clouds are also described correctly by the model.

Some stratiform and cumuliform clouds are misclassified due to an error in texture decision. Using more than four albedos when computing the standard deviations used in the texture test may reduce this error.

Although some large-sized cumuliform clouds are identified by the model, small cumulus are not distinguished by the model; they are classified as clear skies. Since they fail to fill the instrument's field of view, surface radiation reaches the sensor causing a misclassification. Direct pixel-station comparison statistics are better than the 7 x 7 voting procedure results with cumuliform clouds.

Some dense cirrus are analyzed correctly by the model but semitransparent cirrus are not detected by the model and are identified as clear skies or low clouds. Again, surface radiation influences the cloud-typing decision.

Most cumulus congestus clouds are analyzed as cumulus since the infrared temperatures are warmer than the threshold used to separate cumulus congestus from cumulus. It is probable that the majority of these reports of cumulus congestus are analyzed correctly as cumulus since they are ship observations; cumulus congestus is more likely to exist over land than water.

Cumulonimbus are classified incorrectly as cumulus, cumulus congestus or nimbostratus since the infrared temperatures and visible albedos are too warm and/or too dim, respectively, to result in the cumulonimbus classification.

The cloud-top temperature/height analyses are generally accurate. The model is able to depict the wide range of temperatures/heights associated with the various cloud types of a frontal zone.

The NPS model produces fair analyses of precipitation distribution. Some areas of precipitation are not identified by the model since the visible and/or infrared values are below the precipitation/no precipitation thresholds. Some nonprecipitating regions are identified as precipitating areas since the visible and/or infrared values are above the precipitation/no precipitation thresholds.

Some error in estimating precipitation intensity exists. Many times the intensity is underestimated. This is a difficult quantity to measure using digital satellite data.

Discrepancies between the surface and satellite data may be caused by the difference in perspective between the ground and satellite, alignment of the cloud to the surface stations and misleading WMO code descriptions. Many surface reports of dense low clouds are classified as nimbostratus (multi-layered) by the model. The surface observer cannot see beyond the lowest cloud layer. The satellite sees the top of the cloud structure. An observer views clouds subjectively at different angles for variable areal regions. A satellite interprets objectively the infrared and visible information at a single point. Therefore, problems occur with direct comparison of satellite pixel information and surface observations.

Many times clouds are located on edges of synoptic stations which leads to surface-satellite disagreement. Navigation error may also contribute to this misalignment.

Some of the WMO code descriptions combine several cloud types under one category (i.e. middle cloud WMO code 7) which contributes to subjective cloud interpretation differences.

Recommendations for future research include the following: (1) differentiating between snow cover and clouds by implementing a spectral and spatial scheme (Tsonis, 1984) that separates classes of cloud and surface characteristics; (2) using more than four points when computing cloud amount and standard deviations used in the texture test which may reduce the broken and scattered and stratiform/cumuliform classification errors; (3) optimizing the model so that coarser visible and infrared resolution can be used to produce cloud and precipitation analyses; (4) further testing of the threshold values using GOES data from different geographical regions; (5) utilizing digitized GOES-TAP data as input compared to stretched digital VISSR data with the NPS model.

APPENDIX A

TABLES

TABLE 1

WMO Low Cloud Types

Code Figure	Specification
0	No Stratocumulus, Stratus, Cumulus, or Cumulonimbus
1	Cumulus humulis or Cumulus fractus other than that of bad weather, or both
2	Cumulus mediocris or congestus, with or without Cumulus of specis fractus or humulis or Stratocumulus, all having their bases at the same level
3	Cumulonimbus calvus, with or without Cumulus, Stratocumulus or Stratus
4	Stratocumulus cumulogenitus
5	Stratocumulus other than Stratocumulus cumulogenitus
6	Stratus nebulosus or Stratus fractus other than that of bad weather, or both
7	Stratus fractus or Cumulus fractus of bad weather, or both (pannus), usually below Altostratus or Nimbostratus
8	Cumulus and Stratocumulus other than Stratocumulus cumulogenitus, with bases at different levels
9	Cumulonimbus capillatus (often with an anvil) with or without Cumulonimbus calvus, Cumulus, Stratocumulus, Stratus or pannus

TABLE 2

WMO Middle Cloud Types

Code Figure	Specification
0	No Altocumulus, Altostratus or Nimbostratus
1	Altostratus translucidus
2	Altostratus opacus or Nimbostratus
3	Altocumulus translucidus at a single level
4	Patches (often lenticular) of Altocumulus translucidus, continually changing and occurring at one or more levels
5	Altocumulus translucidus in bands, or one or more layers of Altocumulus translucidus or opacus, progressively invading the sky; these Altocumulus clouds generally thicken as a whole
6	Altocumulus cumulogenitus (or cumulonimbogenitus)
7	Altocumulus translucidus or opacus in two or more layers, or Altocumulus opacus in a single layer, not progressively invading the sky, or Altocumulus with Altostratus or Nimbostratus
8	Altocumulus castellanus or floccus
9	Altocumulus of a chaotic sky, generally at several levels

TABLE 3

WMO High Cloud Types

Code Figure	Specification
0	No Cirrus, Cirrocumulus or Cirrostratus
1	Cirrus fibratus, sometimes uncinus, not progressively invading the sky
2	Cirrus spissatus, in patches or entangled sheaves, which usually do not increase and sometimes seem to be the remains of the upper part of a Cumulonimbus; or castellanus or floccus
3	Cirrus spissatus cumulonimbogenitus
4	Cirrus uncinus or fibratus, or both, progressively invading the sky; they generally thicken as a whole
5	Cirrus (often in bands)and Cirrostratus, or Cirrostratus alone, progressively invading the sky; they generally thicken as a whole, but the continuous veil extends more than 45 degrees above the horizon
6	Cirrus (often in bands)and Cirrostratus, or Cirrostratus alone, progressively invading the sky; they generally thicken as a whole, but the continuous veil extends more than 45 degrees above the horizon, without the sky being totally covered
7	Cirrostratus covering the whole sky
8	Cirrostratus not progressively invading the sky and not entirely covering it
9	Cirrocumulus alone, or Cirrocumulus predominant among the high clouds

TABLE 4

Specific Cloud Type Statistics for Initial Cases

	Direct Comparison	7 x 7 Vote	Direct Comparison	7 x 7 Vote
	17 Jan		20 Mar	
Clr	4/4 (100%)	4/4 (100%)	19/21 (90%)	19/21 (90%)
Ci	no report	no report	2/11 (18%)	1/11
As	0/1	0/1	0/1	0/1
St	2/8 (25%)	1/8 (13%)	no report	no report
Sc	10/25 (40%)	14/25 (56%)	1/5 (20%)	1/5 (20%)
Ns	6/21 (29%)	8/21 (38%)	no report	no report
Cu	0/4	0/4	1/4 (25%)	1/4 (25%)
CC	0/1	0/1	0/3	0/3
Cb	no report	no report	no report	no report
	28 Mar		11 Apr	
Clr	9/10 (90%)	9/10 (90%)	5/7 (71%)	6/7 (86%)
Ci	1/1 (100%)	1/1 (100%)	0/5	0/5
As	no report	no report	no report	no report
St	0/2	0/2	0/1	0/1
Sc	8/20 (40%)	11/20 (55%)	5/14 (36%)	6/14 (43%)
Ns	4/7 (57%)	4/7 (57%)	no report	no report
Cu	3/5 (60%)	2/5 (40%)	0/4	0/4
CC	0/2	0/2	0/1	0/1
Cb	no report	no report	no report	no report
	13 May		Total for all cases	
Clr	24/25 (96%)	25/25 (100%)	61/67 (91%)	63/67 (94%)
Ci	1/6 (17%)	1/6 (17%)	4/23 (17%)	3/23 (13%)
As	no report	no report	0/2	0/2
St	0/1	0/1	2/12 (17%)	1/12
Sc	0/1	0/1	24/65 (37%)	32/65 (49%)
Ns	no report	no report	10/28 (36%)	12/28 (43%)
Cu	1/3 (33%)	1/3 (33%)	5/20 (25%)	4/20 (20%)
CC	0/9	0/9	0/16	0/16
Cb	0/1	0/1	0/1	0/1

TABLE 5

Cloud Group Statistics for Initial Cases

	Direct Comparison	7 x 7 Vote
17 Jan		
Clr	4/4 (100%)	4/4 (100%)
CH	no report	no report
CM	11/22 (50%)	10/22 (45%)
CL	24/38 (63%)	25/38 (66%)
CB	no report	no report
20 Mar		
Clr	19/21 (90%)	19/21 (90%)
CH	1/11	1/11
CM	0/1	0/1
CL	5/12 (42%)	4/12 (33%)
CB	no report	no report
28 Mar		
Clr	9/10 (90%)	9/10 (90%)
CH	1/1 (100%)	1/1 (100%)
CM	5/7 (71%)	4/7 (57%)
CL	19/29 (66%)	19/29 (66%)
CB	no report	no report
11 Apr		
Clr	5/7 (71%)	5/7 (71%)
CH	0/5	0/5
CM	no report	no report
CL	10/20 (50%)	10/20 (50%)
CB	no report	no report
13 May		
Clr	24/25 (96%)	25/25 (100%)
CH	1/6 (17%)	1/6 (17%)
CM	no report	no report
CL	4/14 (29%)	5/14 (36%)
CB	0/1	0/1
Total for all cases		
Clr	61/67 (91%)	63/67 (94%)
CH	4/23 (17%)	3/23 (13%)
CM	16/30 (53%)	14/30 (47%)
CL	62/113 (55%)	63/113 (56%)
CB	0/1	0/1

TABLE 6

Multi-layered Cloud Statistics for Initial Cases

	17 Jan		
Percentage satellite-surface agreement	15/17 (88%)	THIN	2/17
		CH	3/17
		CM	1/17
Percentage satellite-surface mismatched	2/17 (12%)	CL	2/17
		MULTI	7/17
	20 Mar		
Percentage satellite-surface agreement	18/20 (90%)	THIN	3/20
		CH	3/20
		CM	0/20
Percentage satellite-surface mismatched	2/20 (10%)	CL	3/20
		MULTI	9/20
	28 Mar		
Percentage satellite-surface agreement	17/19 (89%)	THIN	6/19
		CH	2/19
		CM	1/19
Percentage satellite-surface mismatched	2/19 (11%)	CL	4/19
		MULTI	4/19
	Apr 11		
Percentage satellite-surface agreement	30/33 (91%)	THIN	6/33
		CH	8/33
		CM	1/33
Percentage satellite-surface mismatched	3/33 (9%)	CL	4/33
		MULTI	11/33
	13 May		
Percentage satellite-surface agreement	18/21 (86%)	THIN	9/21
		CH	4/21
		CM	1/21
Percentage satellite-surface mismatched	3/21 (14%)	CL	1/21
		MULTI	3/21
	Total for all cases		
Percentage satellite-surface agreement	98/110 (89%)	THIN	26/110
		CH	20/110
		CM	4/110
Percentage satellite-surface mismatched	12/110 (11%)	CL	14/110
		MULTI	34/110

TABLE 7

Precipitation Statistics for Initial Cases

17 Jan	
PRECIPITATION	9/22 (41%)
NO PRECIPITATION	54/60 (90%)
20 Mar	
PRECIPITATION	no rain
NO PRECIPITATION	61/65 (94%)
28 Mar	
PRECIPITATION	7/11 (64%)
NO PRECIPITATION	50/55 (91%)
11 Apr	
PRECIPITATION	2/3 (67%)
NO PRECIPITATION	64/68 (94%)
13 May	
PRECIPITATION	1/1 (100%)
NO PRECIPITATION	65/67 (97%)
Total for all cases	
PRECIPITATION	18/37 (49%)
NO PRECIPITATION	295/315 (94%)

TABLE 8

Specific Cloud Type Statistics for Independent Test Cases

	Direct Comparison		7 x 7 Vote
		20 Feb	
Clr	41/65 (63%)		45/65 (69%)
Ci	0/5		0/5
As	no report		no report
St	1/6 (17%)		0/6
Sc	3/10 (30%)		3/10 (30%)
Ns	2/2 (100%)		2/2 (100%)
Cu	no report		no report
CC	no report		no report
Cb	no report		no report
		27 Mar	
Clr	16/17 (94%)		17/17 (100%)
Ci	3/20 (15%)		3/20 (15%)
As	no report		no report
St	0/2		0/2
Sc	4/14 (29%)		4/14 (29%)
Ns	5/6 (83%)		5/6 (83%)
Cu	0/3		1/3 (33%)
CC	0/1		0/1
Cb	no report		no report
		16 Apr	
Clr	19/19 (100%)		19/19 (100%)
Ci	no report		no report
As	no report		no report
St	0/1		0/1
Sc	2/4 (50%)		2/4 (50%)
Ns	1/3 (33%)		1/3 (33%)
Cu	2/5 (40%)		1/5 (20%)
CC	0/6		0/6
Cb	0/4		0/4
		15 May	
Clr	12/12 (100%)		12/12 (100%)
Ci	0/6		0/6
As	0/1		0/1
St	no report		no report
Sc	3/9 (33%)		5/9 (56%)
Ns	1/4 (25%)		1/4 (25%)
Cu	no report		no report
CC	0/6		0/6
Cb	0/1		0/1
		Total for all cases	
Clr	88/113 (78%)		93/113 (82%)
Ci	3/31 (10%)		3/31 (10%)
As	0/1		0/1
St	1/9 (11%)		0/9
Sc	12/37 (32%)		14/37 (38%)
Ns	9/15 (60%)		8/15 (53%)
Cu	2/8 (25%)		2/8 (25%)
CC	0/13		0/13
Cb	0/5		0/5

TABLE 9

Cloud Group Statistics for Independent Test Cases

	Direct Comparison	7 x 7 Vote
	20 Feb	
Clr	41/65 (63%)	45/65 (69%)
CH	0/5	0/5
CM	2/2 (100%)	1/2 (50%)
CL	6/16 (38%)	5/16 (31%)
CB	no report	no report
	27 Mar	
Clr	17/17 (100%)	17/17 (100%)
CH	3/20 (15%)	3/20 (15%)
CM	5/6 (83%)	5/6 (83%)
CL	5/20 (25%)	5/20 (25%)
CB	no report	no report
	16 Apr	
Clr	19/19 (100%)	19/19 (100%)
CH	no report	no report
CM	2/3 (67%)	2/3 (67%)
CL	10/16 (63%)	10/16 (63%)
CB	0/4	0/4
	15 May	
Clr	12/12 (100%)	12/12 (100%)
CH	0/6	0/6
CM	4/5 (80%)	4/5 (80%)
CL	10/15 (67%)	10/15 (67%)
CB	0/1	0/1
	Total for all cases	
Clr	89/113 (79%)	93/113 (82%)
CH	3/31 (10%)	3/31 (10%)
CM	13/16 (81%)	12/16 (75%)
CL	31/67 (46%)	30/67 (45%)
CB	0/5	0/5

TABLE 10

Multi-layered Cloud Statistics for Independent Test Cases

	20 Feb		
Percentage satellite-surface agreement	16/17 (94%)	THIN	5/17
		CH	0/17
		CM	1/17
		CL	7/17
		MULTI	3/17
Percentage satellite-surface mismatched	1/17 (6%)		
	27 Mar		
Percentage satellite-surface agreement	25/28 (89%)	THIN	6/28
		CH	3/28
		CM	0/28
		CL	0/28
		MULTI	16/28
Percentage satellite-surface mismatched	3/28 (11%)		
	16 Apr		
Percentage satellite-surface agreement	20/21 (95%)	THIN	2/21
		CH	0/21
		CM	1/21
		CL	4/21
		MULTI	13/21
Percentage satellite-surface mismatched	1/21 (5%)		
	15 May		
Percentage satellite-surface agreement	20/20 (100%)	THIN	4/20
		CH	1/20
		CM	1/20
		CL	9/20
		MULTI	5/20
Percentage satellite-surface mismatched	0/20		
	Total for all cases		
Percentage satellite-surface agreement	81/86 (94%)	THIN	17/86
		CH	4/86
		CM	3/86
		CL	20/86
		MULTI	37/86
Percentage satellite-surface mismatched	5/86 (6%)		

TABLE 11

Precipitation Statistics for Independent Test Cases

20 Feb	
PRECIPITATION	2/3 (67%)
NO PRECIPITATION	100/102 (98%)
27 Mar	
PRECIPITATION	11/11 (100%)
NO PRECIPITATION	67/80 (84%)
16 Apr	
PRECIPITATION	4/6 (67%)
NO PRECIPITATION	55/57 (96%)
15 May	
PRECIPITATION	3/4 (75%)
NO PRECIPITATION	52/55 (95%)
Total for all cases	
PRECIPITATION	20/24 (83%)
NO PRECIPITATION	274/294 (93%)

APPENDIX B

FIGURES

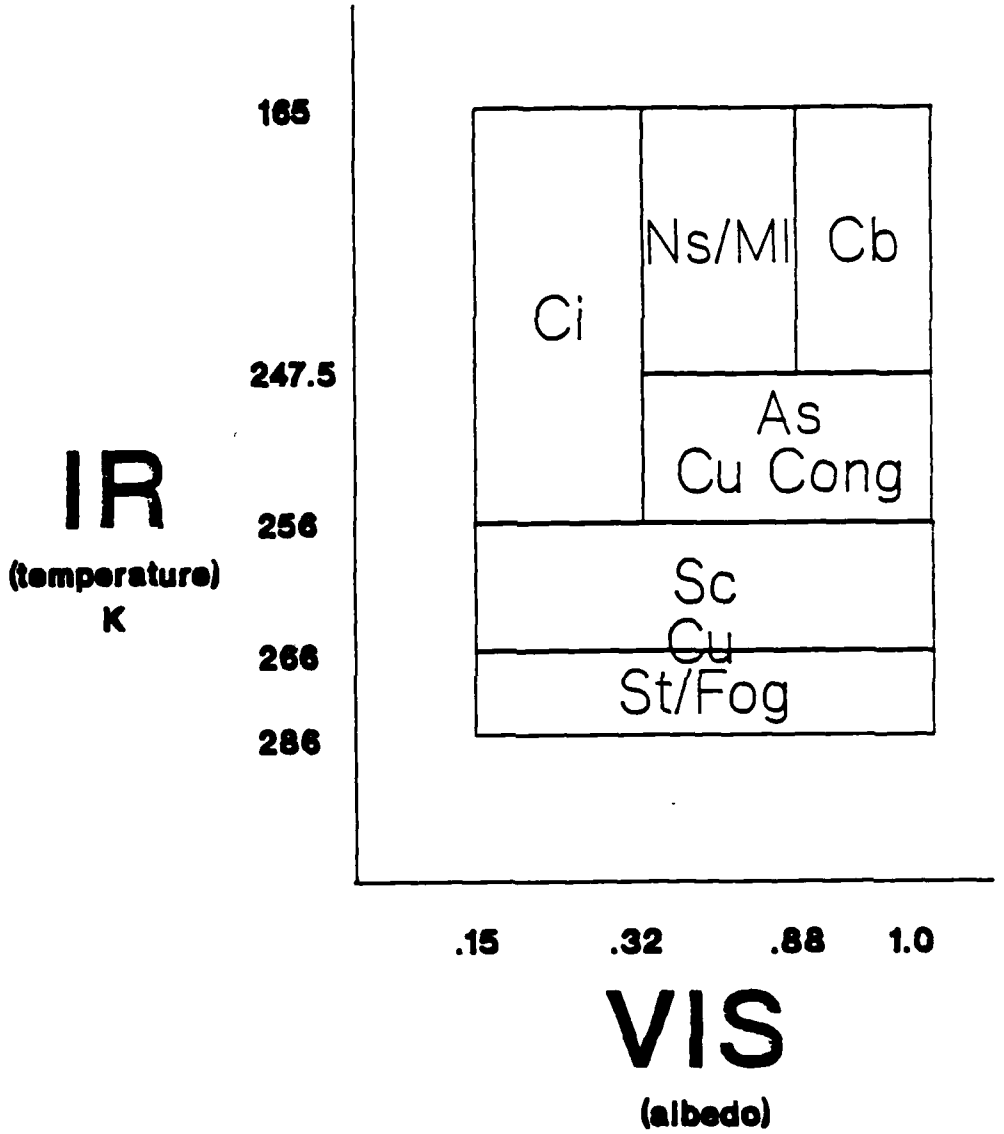

Figure 1. Two-dimensional Cloud-typing Graph Using GOES Infrared and Visible Satellite Digital Data for 17 Jan 85

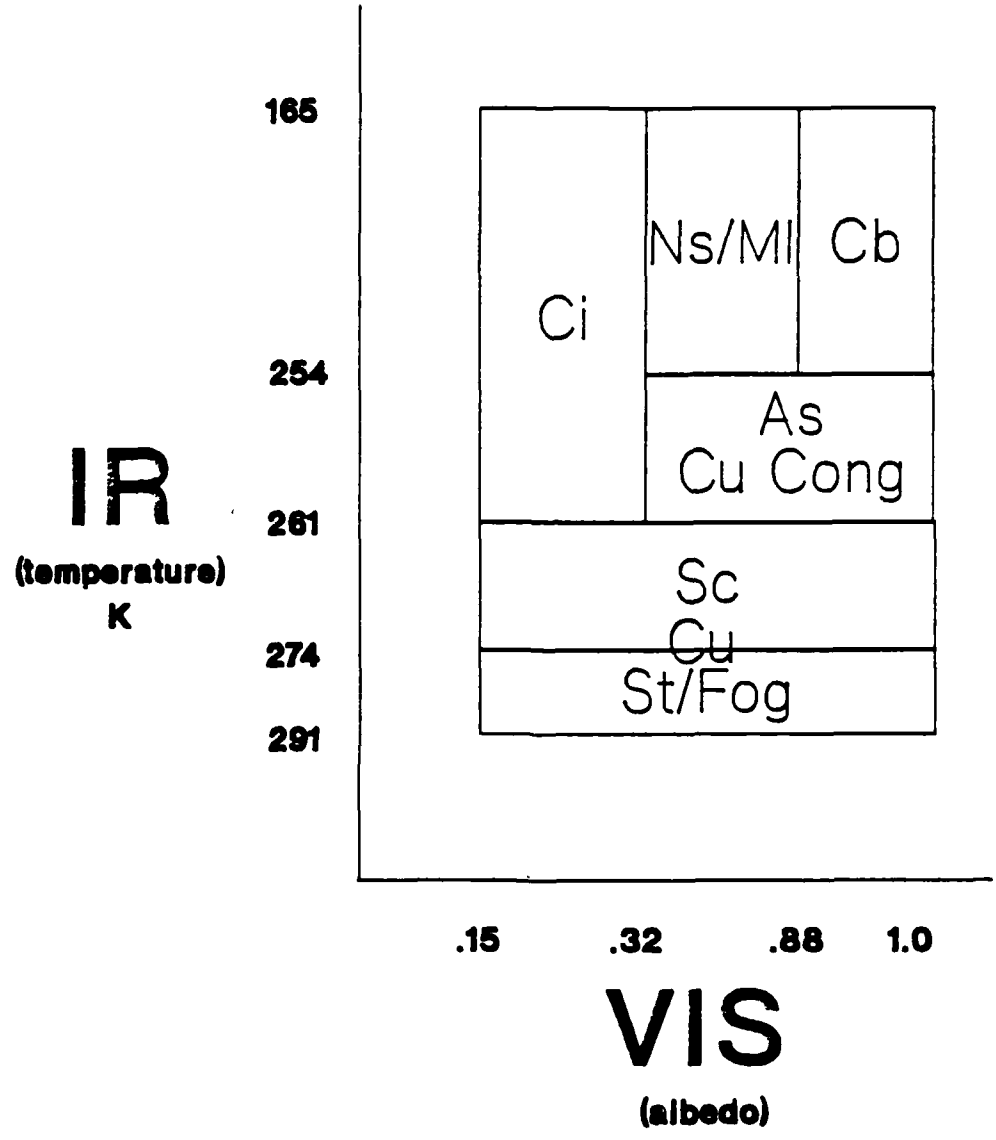

Figure 2. Two-dimensional Cloud-typing Graph Using GOES Infrared and Visible Satellite Digital Data for 20 Mar 85

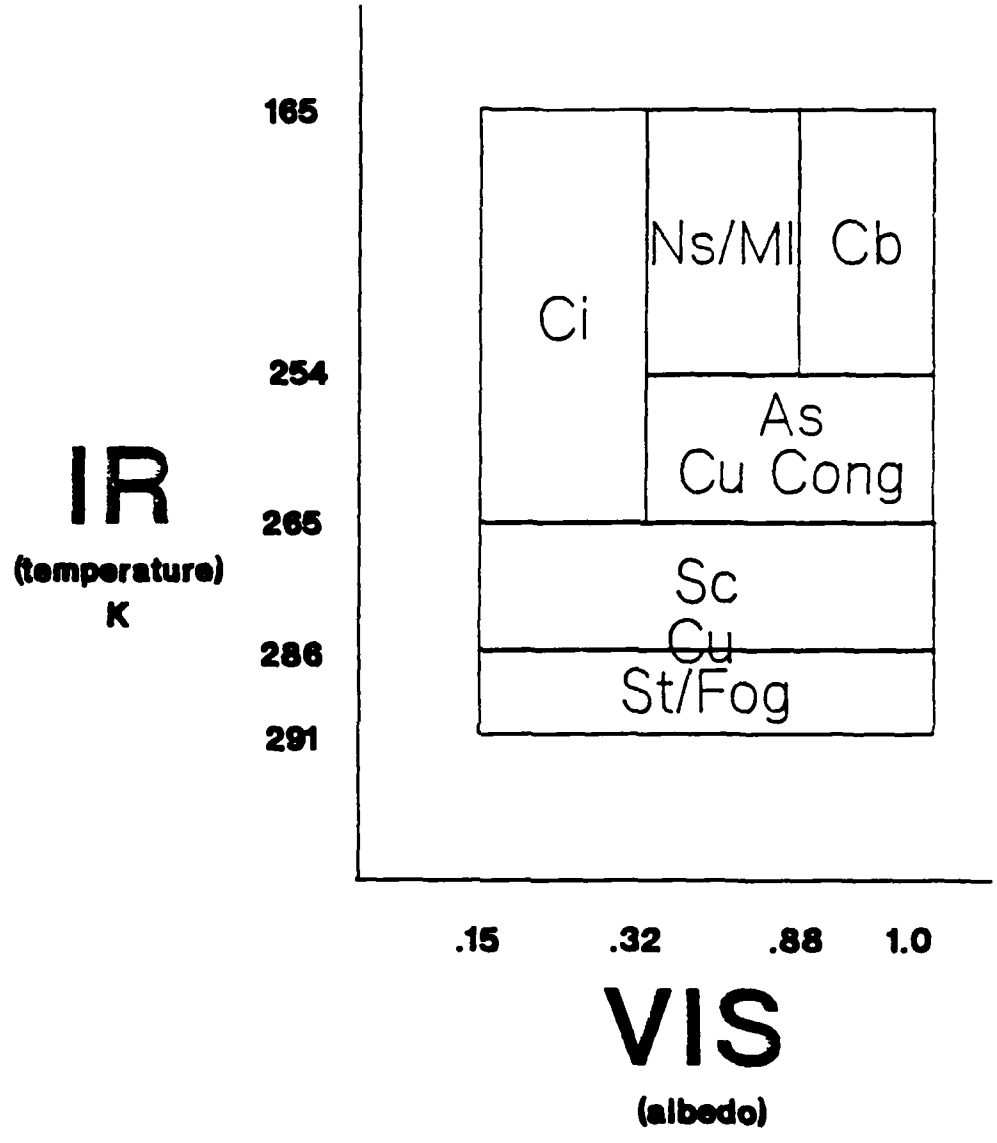

Figure 3. Two-dimensional Cloud-typing Graph Using GOES Infrared and Visible Satellite Digital Data for 28 Mar 85

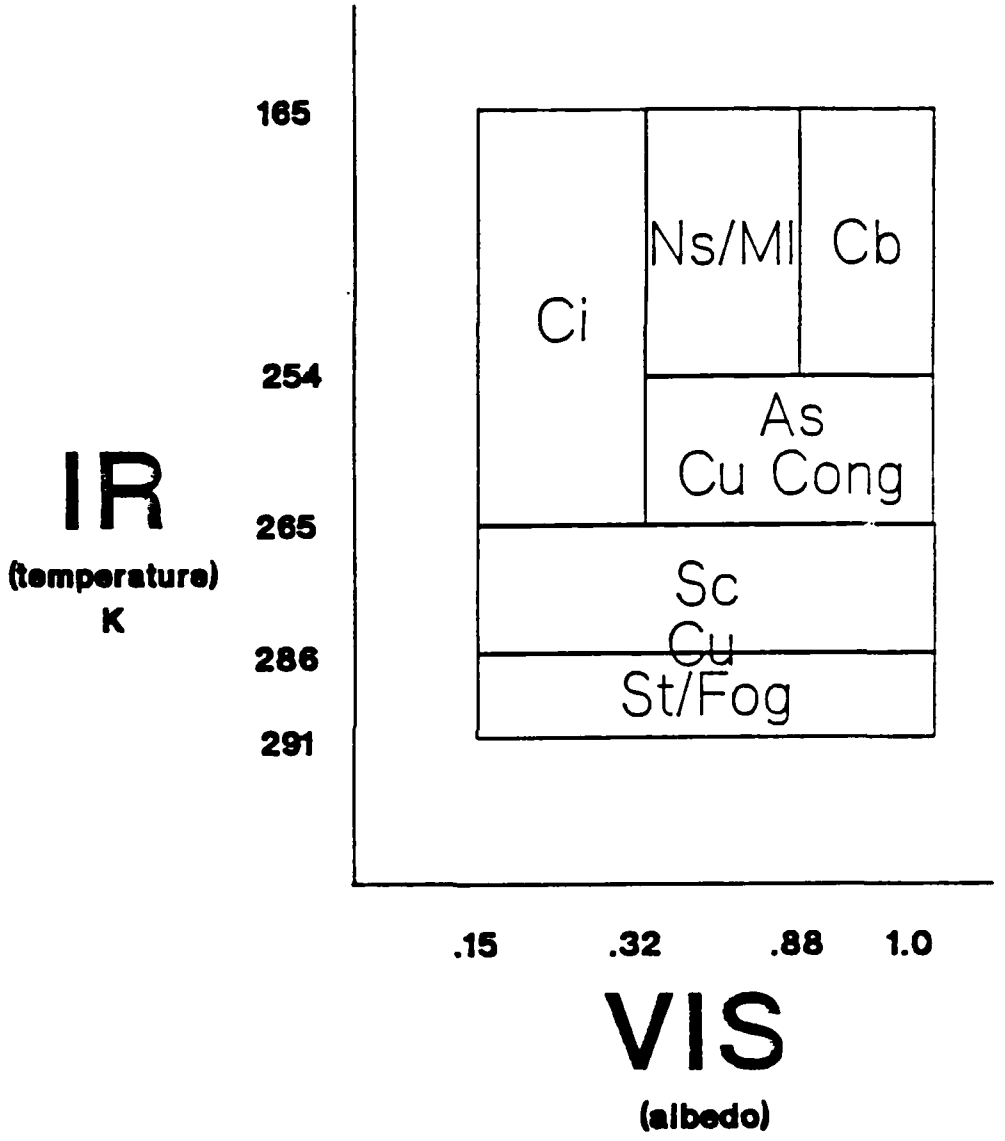

Figure 4. Two-dimensional Cloud-typing Graph Using GOES Infrared and Visible Satellite Digital Data for 11 Apr 85

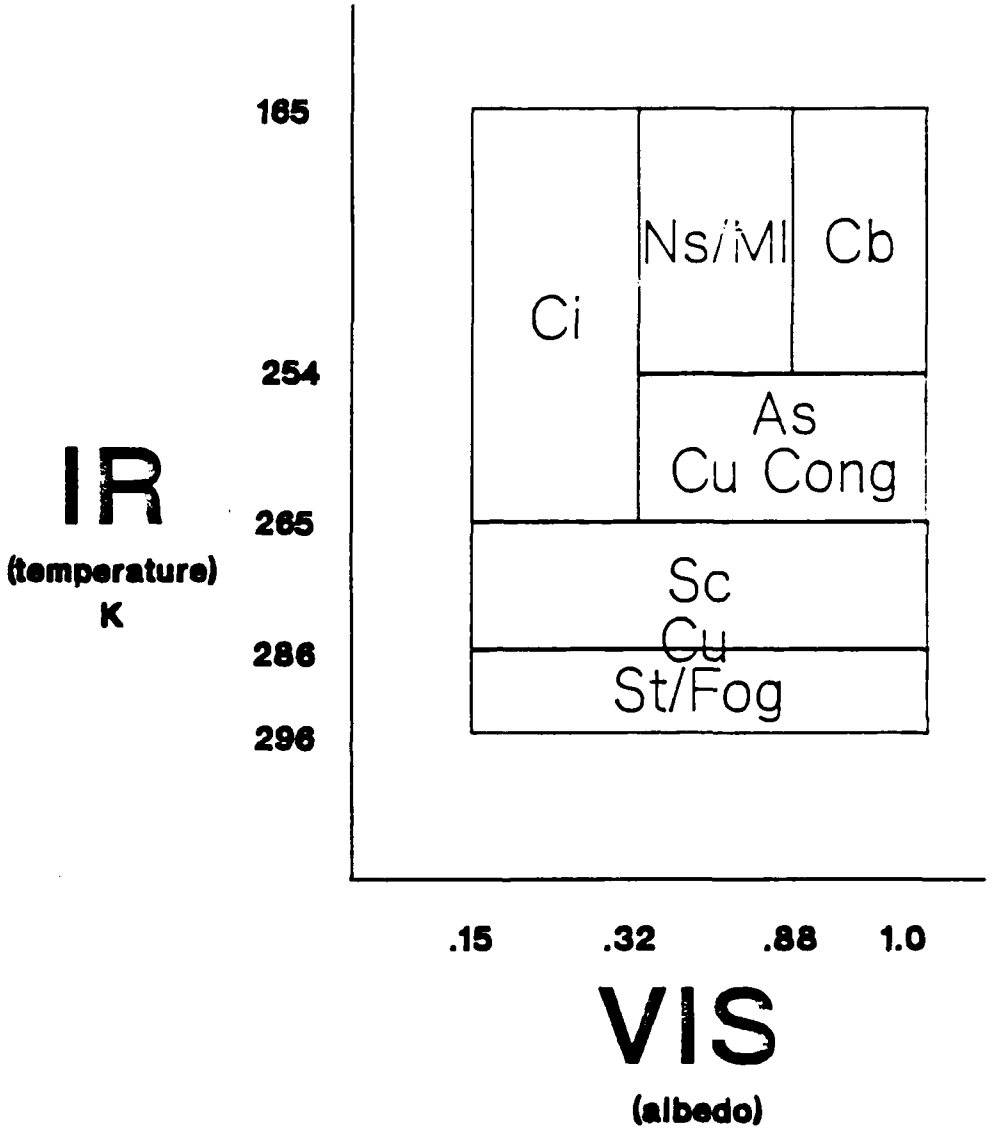

Figure 5. Two-dimensional Cloud-typing Graph Using GOES Infrared and Visible Satellite Digital Data for 13 May 85

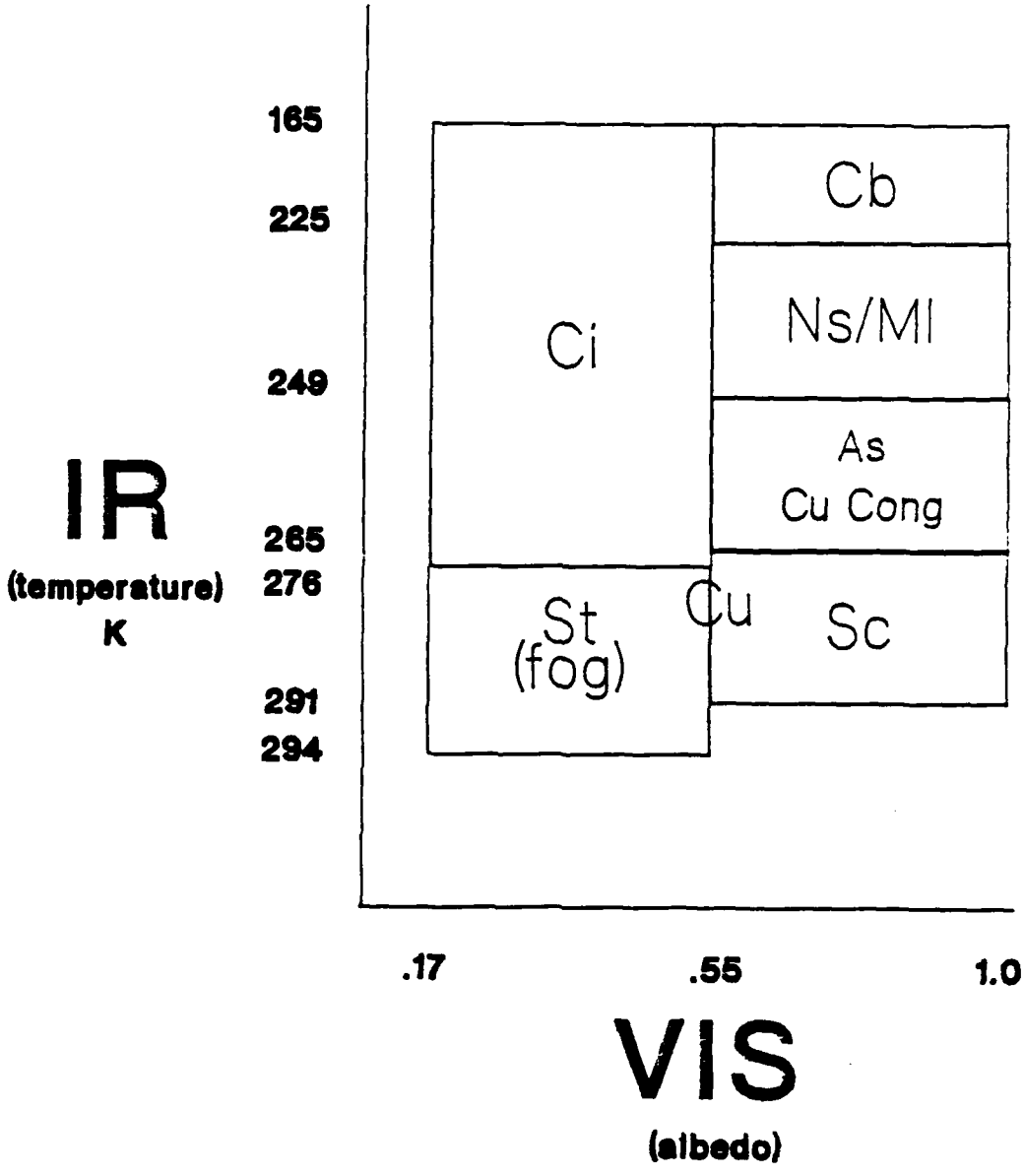

Figure 6. Two-dimensional Cloud-typing Graph Using GOES Infrared and Visible Satellite Digital Data for Summer 83

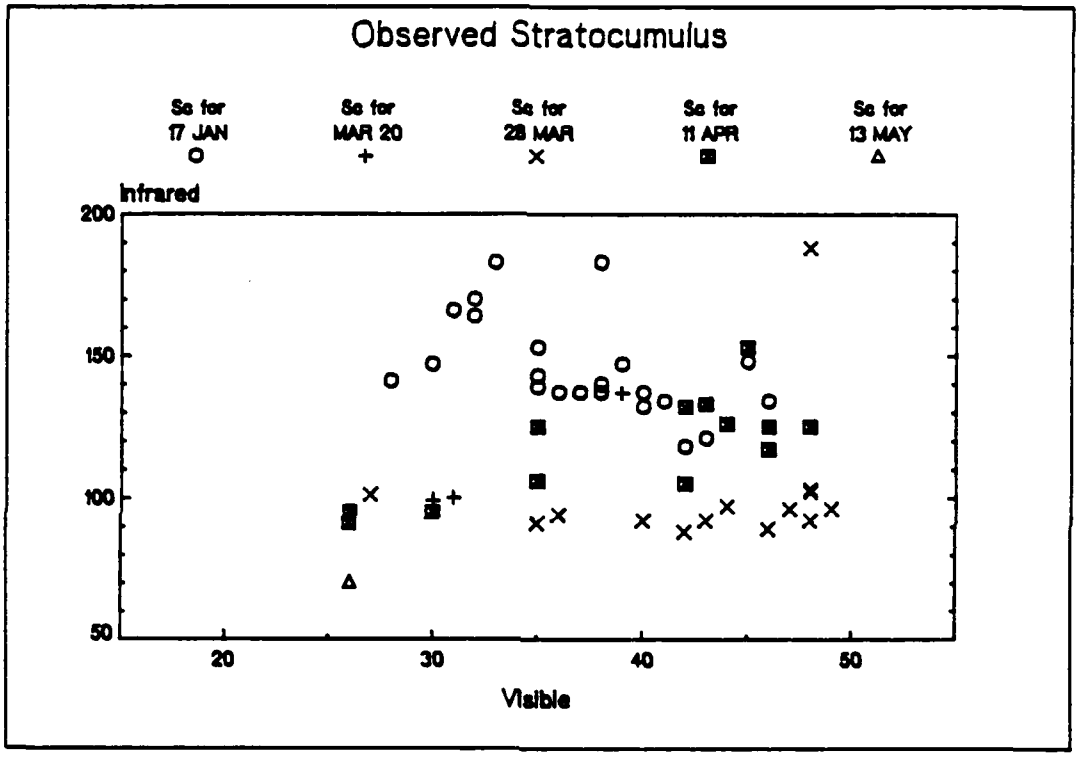

Figure 7. Scattergram of Visible and Infrared Raw Data Counts Corresponding to Surface Reports of Stratocumulus (Lower Infrared Count for Warmer Temperature)

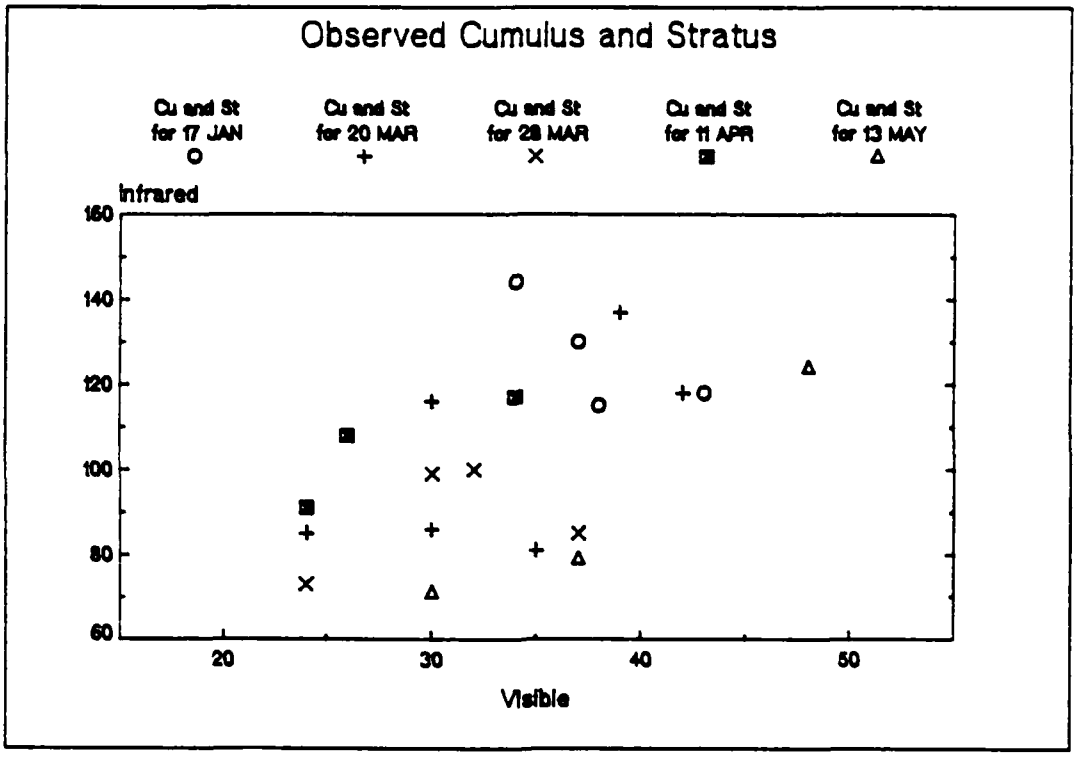

Figure 8. Scattergram of Visible and Infrared Raw Data Counts Corresponding to Surface Reports of Cumulus and Stratus (Lower Infrared Count for Warmer Temperature)

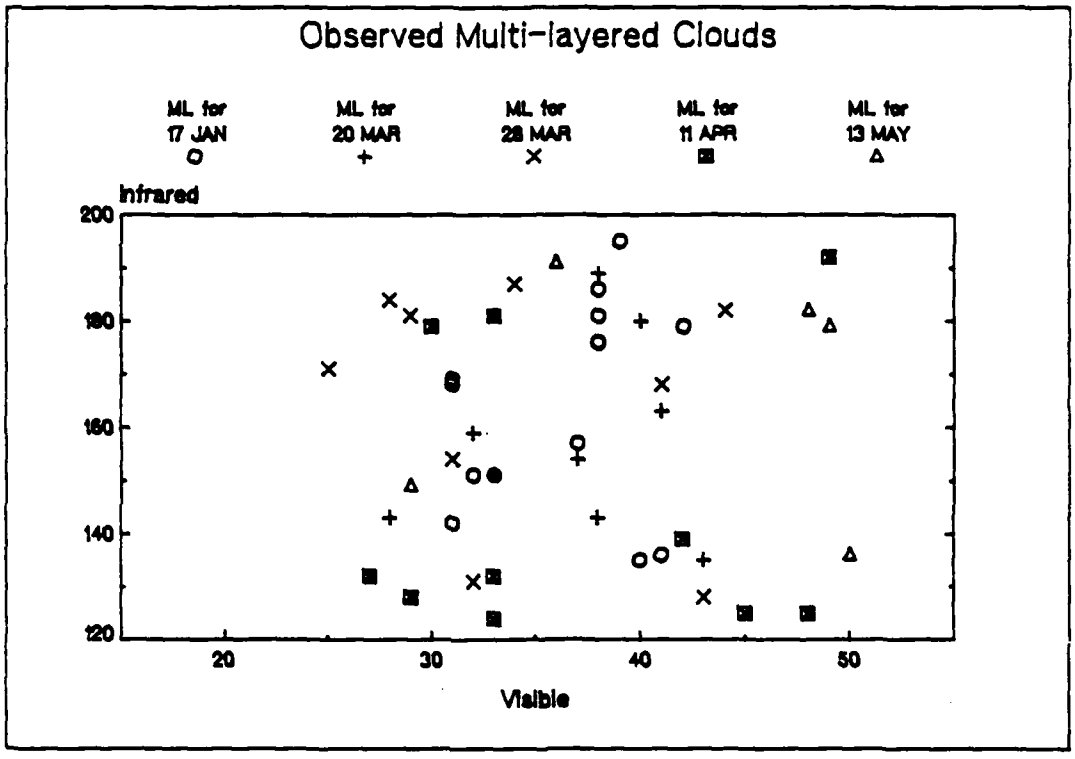

Figure 9. Scattergram of Visible and Infrared Raw Data Counts Corresponding to Surface Reports of Multi-layered Clouds (Lower Infrared Count for Warmer Temperature)

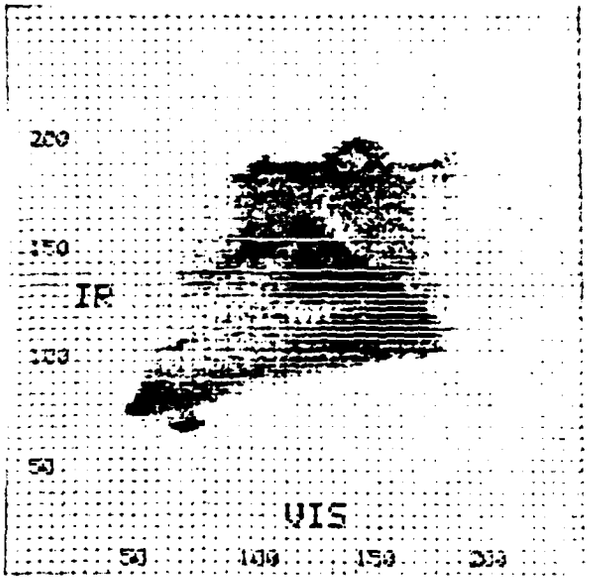

Figure 10. Two-dimensional Frequency Graph Using GOES Infrared and Visible Satellite Digital Data for 17 Jan 85. The Number in the Darkened Regions Represents the Average Frequency of Occurrence (Higher Frequency in Darker Areas) of Each Infrared and Visible (Scaled to Infrared Data by Mulitplying by Four) Count Combination That Occurs Within the Image

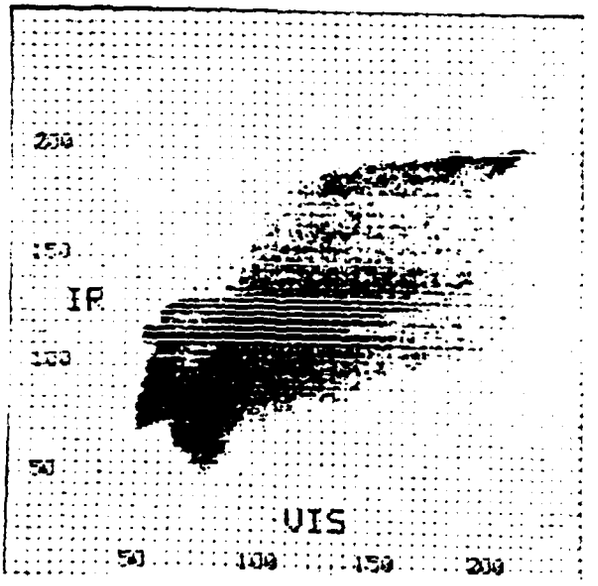

Figure 11. Same as Fig. 10 except for 20 Mar 85

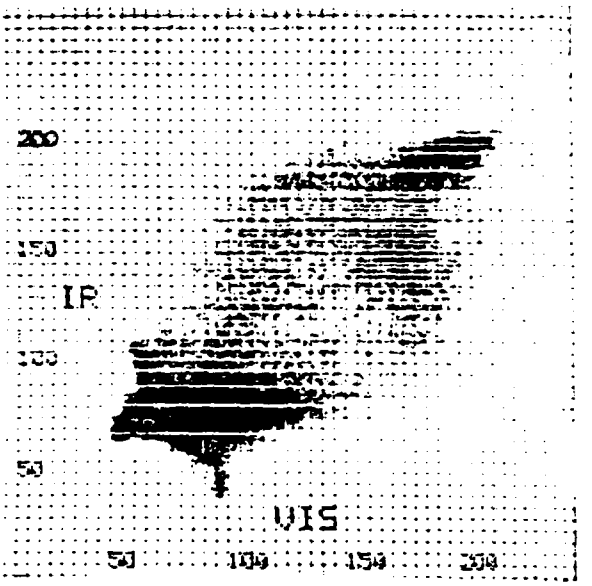

Figure 12. Same as Fig. 10 except for 13 May 85

Figure 13. GOES Visual Imagery for 1800 GMT Jan 85

Figure 14. GOES Infrared Imagery for 1800 GMT 17 Jan 85

Figure 15. Cloud Amount Analysis for 1800 GMT 17 Jan 85. Four Colors Are Used To Distinguish Between Cloud Amounts: 100% Cloud Cover (OVC), Blue; 75% Cloud Cover (BRO/OVC), Dark Green; 50% Cloud Cover (BRO), Light Green; 25% Cloud Cover (SCA), Red

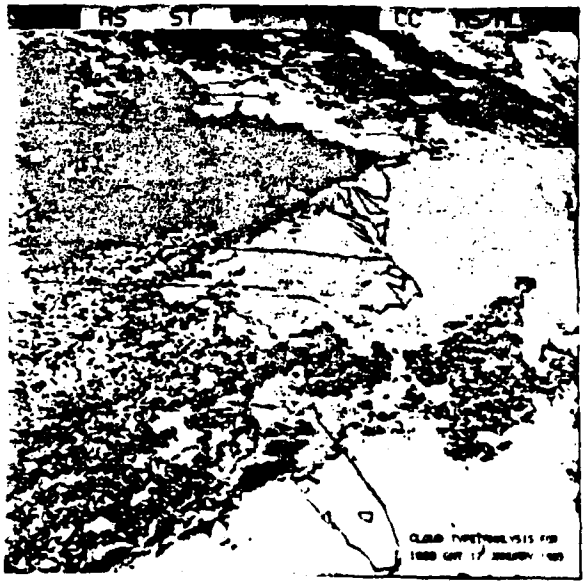

Figure 16. Cloud Type Analysis for 1800 GMT 17 Jan 85. Eight Colors Are Used To Illustrate Eight Different Cloud Type Cumulonimbus (Cb), Dark Blue; Nimbostratus (Ns), Blue; Cumulus Congestus (CC), Light Blue; Cumulus (Cu), Dark Green; Stratocumulus (Sc), Light Green; Stratus (St), Yellow; Altostratus (As), Orange; Cirrus (Ci), Red

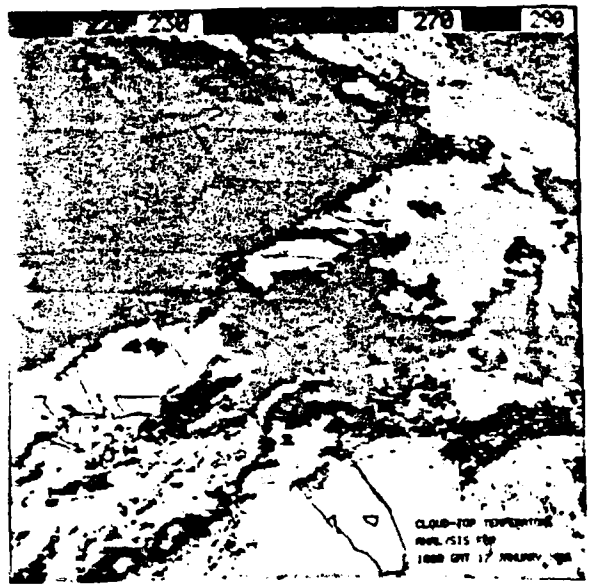

Figure 17. Cloud-top Temperature Analysis for 1800 GMT 17 Jan. Nine Colors Are Used To Illustrate 10 K Intervals of Cloud-top Temperatures: 210-219 K, Dark Blue; 220-229 K, Blue; 230-239 K, Light Blue; 240-249 K, Dark Green; 250-259 K Green; 260-269 K, Light Green; 270-279 K, Yello 280-289 K, Red; 290-300 K (surface), Gray

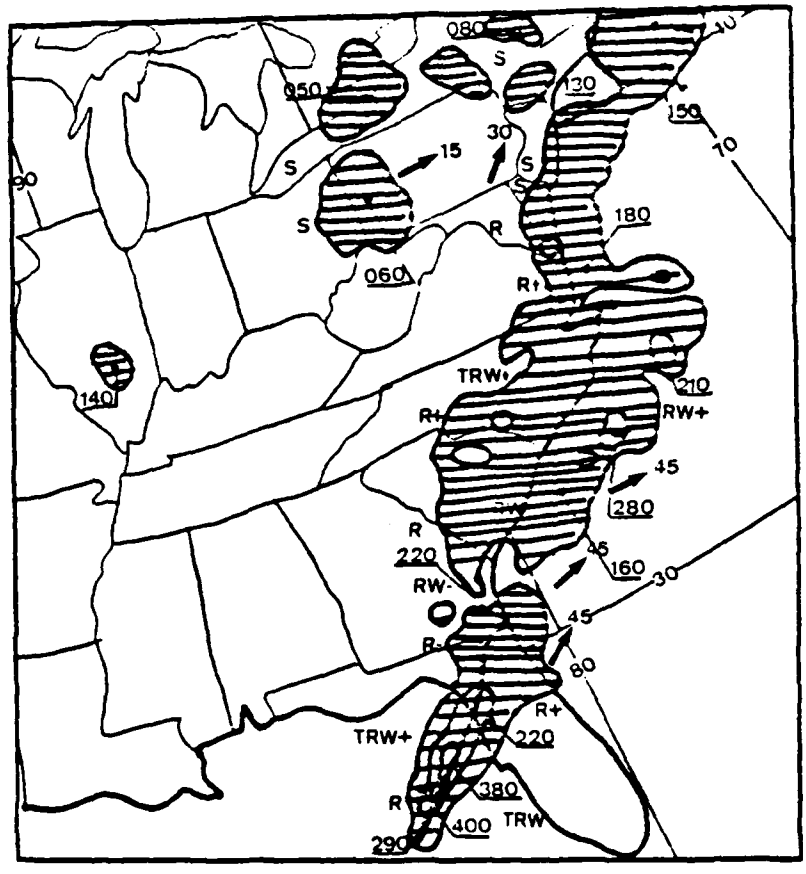

Figure 18. Automated Radar Summary Chart for 17 JAN 85

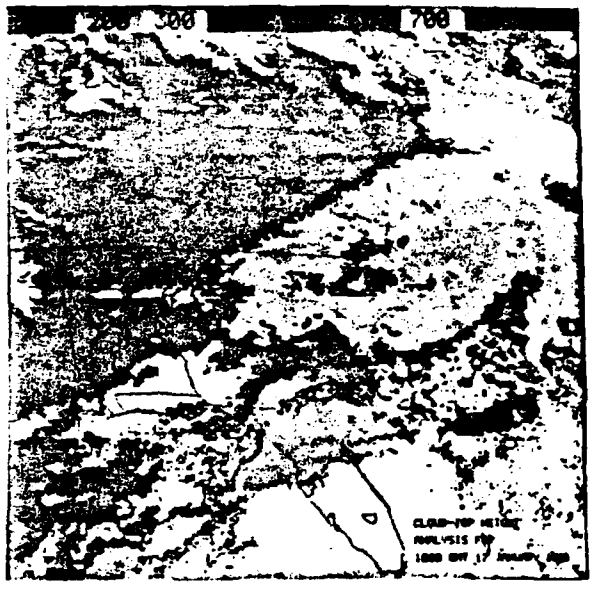

Figure 19. Cloud-top Height Analysis for 1800 17 Jan 85. Nine Colors Are Used To Illustrate 100 mb Cloud-top Height Intervals: 100-199 mb, Dark Blue; 200-299 mb, Blue; 300-399 mb, Light Blue; 400-499 mb, Dark Green; 500-599 mb, Green; 600-699 mb, Light Green; 700-799 mb, Yellow; 800-899 mb, Red; 900-1000 mb, Dark Red

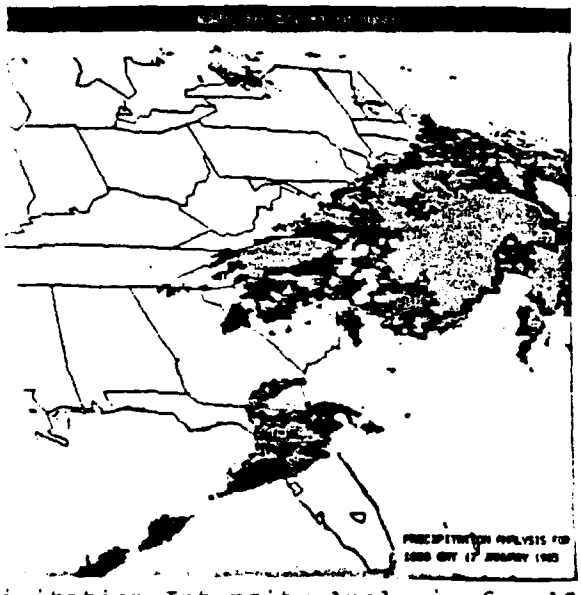

Figure 20. Precipitation Intensity Analysis for 1800 GMT 17 Jan 85. Three Colors Are Used To Distinguish Between Precipitation Intensities: Light, Red; Moderate, Green; Heavy, Blue

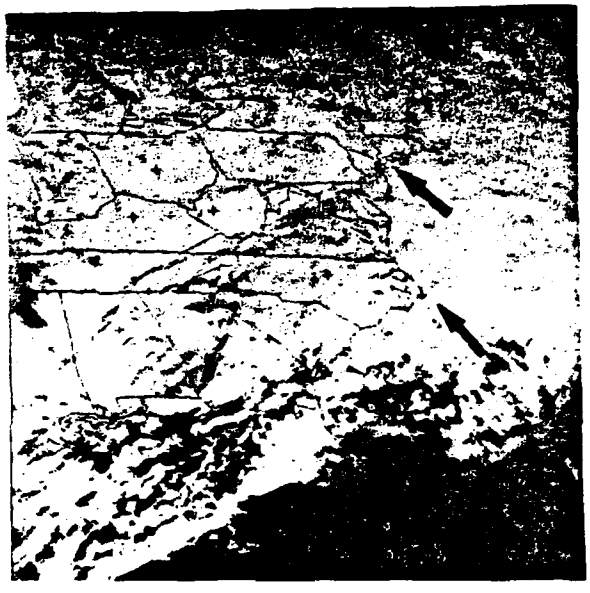

Figure 21. Synoptic Surface Station Observations of WMO Cloud Types and Present Weather Over GOES Visible Imagery for 1800 GMT 17 Jan 85. The Number In the Upper Left Corner Is the WMO Low Cloud Type; the Number In the Lower Left Corner Is the WMO Middle Cloud Type; and the Number In the Upper Right Corner Is the WMO High Cloud Type. Standard WMO Weather Abbreviations Are Found In the Lower Right Corner.

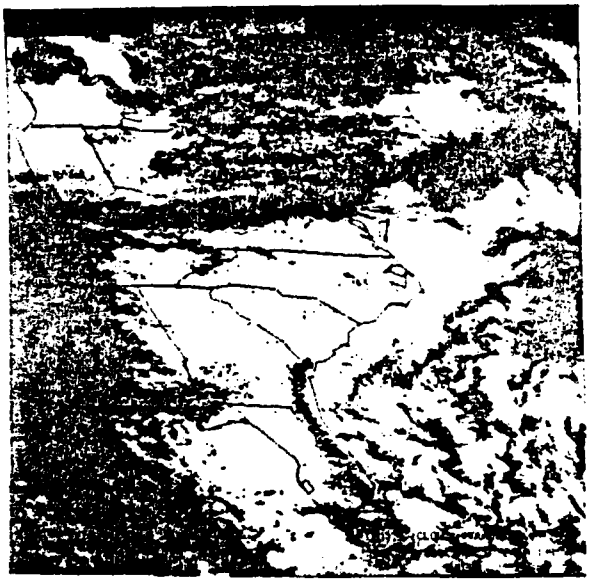

Figure 22. Same as Fig. 15 except for 20 Mar 85

Figure 23. GOES Visible Imagery for 20 Mar 85

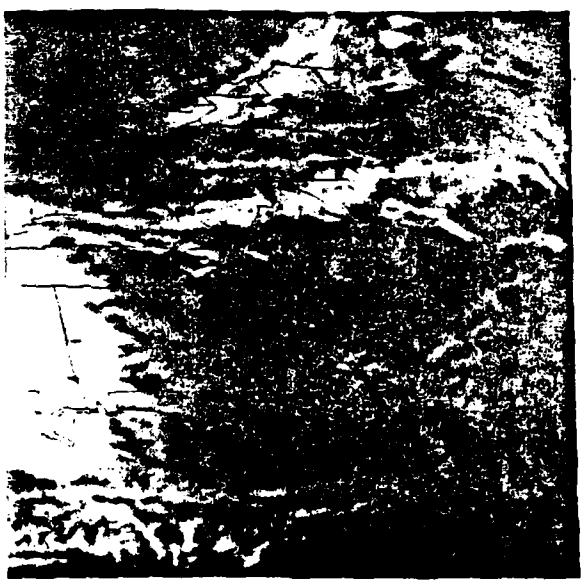

Figure 24. GOES Infrared Imagery for 20 Mar 85

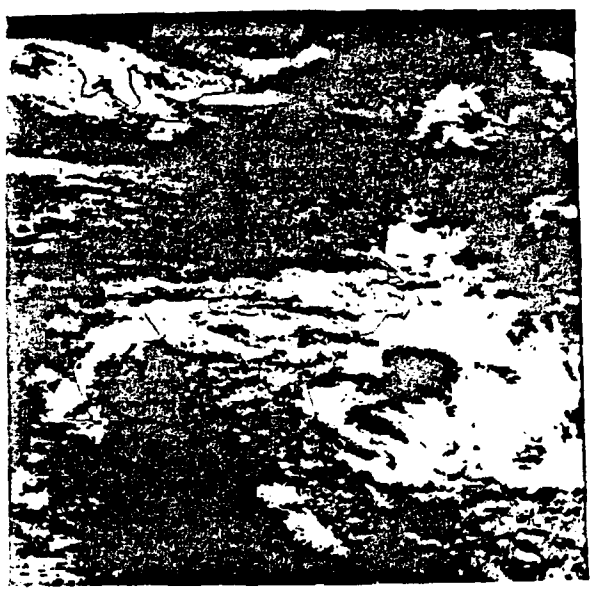

Figure 25. Same as Fig. 15 except for 11 Apr 85

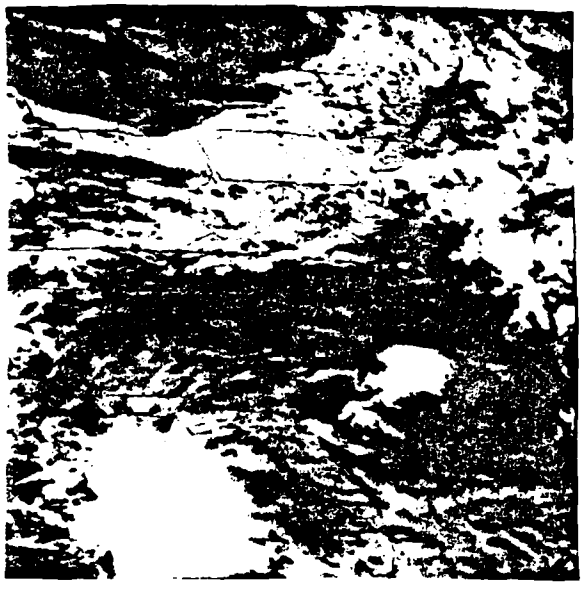

Figure 26. GOES Visible Imagery for 11 Apr 85

Figure 27. GOES Infrared Imagery for 11 Apr 85

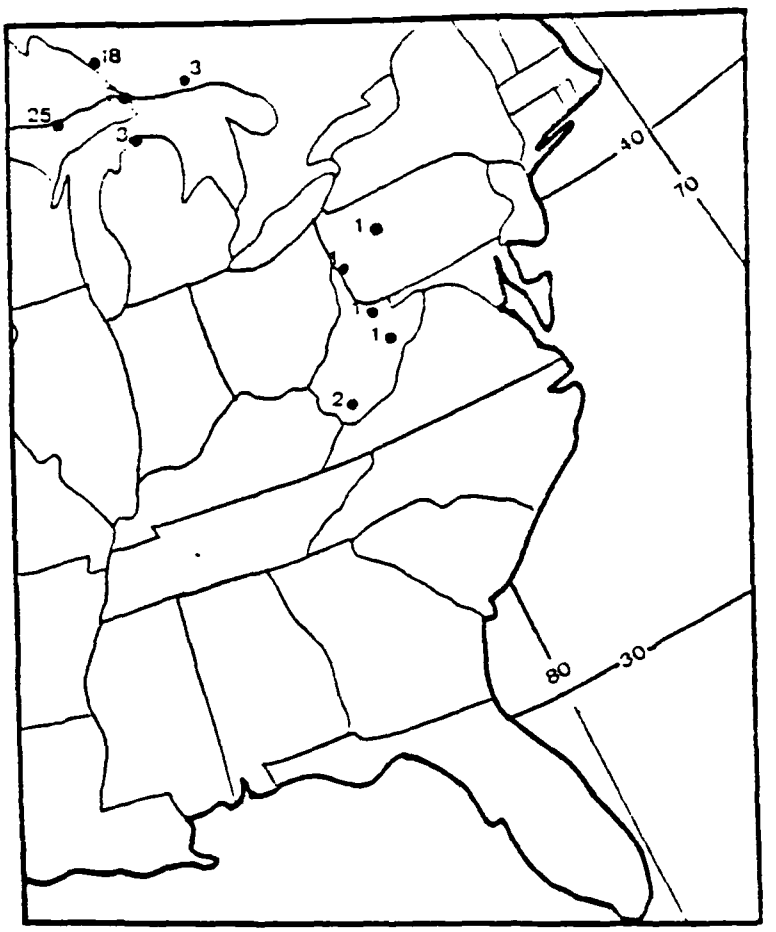

Figure 28. Snow Cover In Inches for 1200 GMT 10 Apr 85

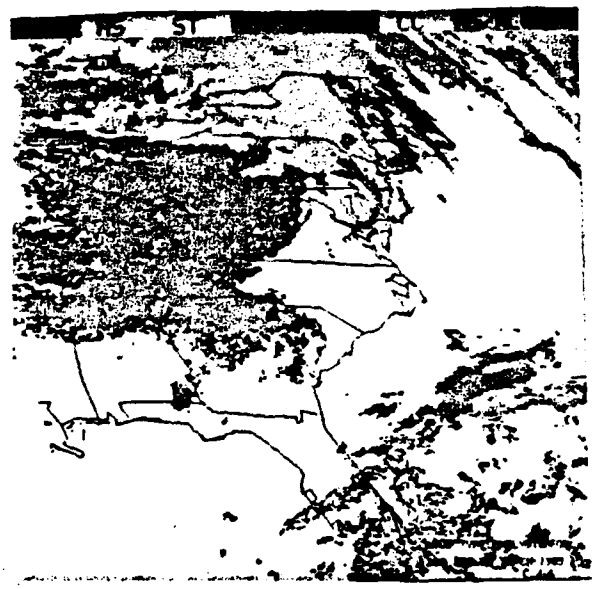

Figure 29. Same as Fig. 16 except for 28 Mar 85

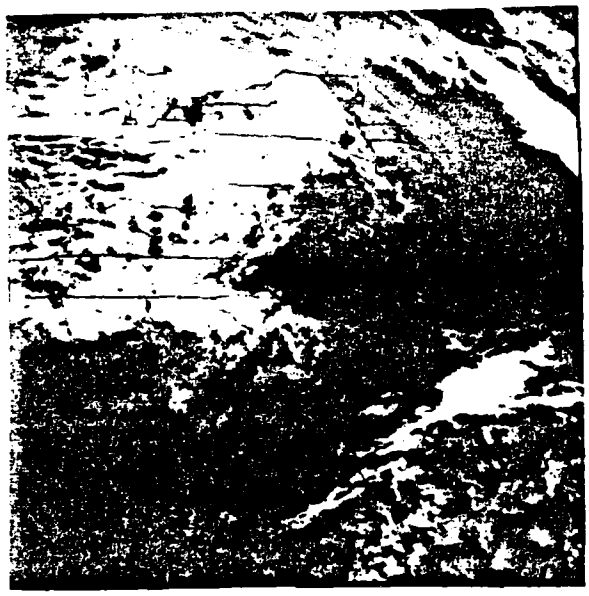

Figure 30. GOES Visible Imagery for 28 Mar 85

Figure 31. GOES Infrared Imagery for 28 Mar 85

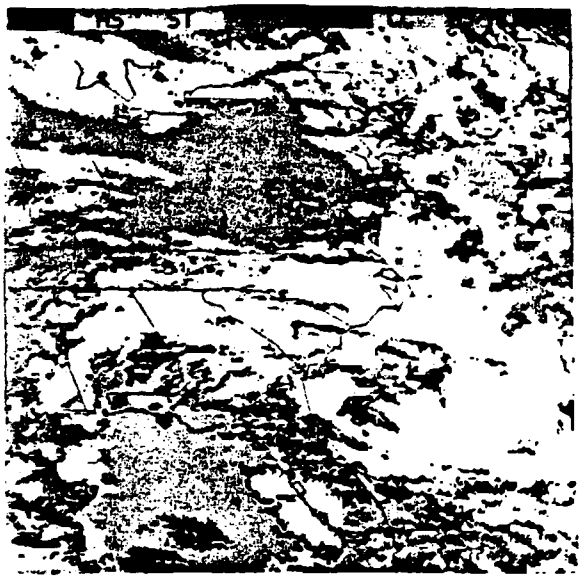

Figure 32. Same as Fig. 16 except for 11 Apr 85

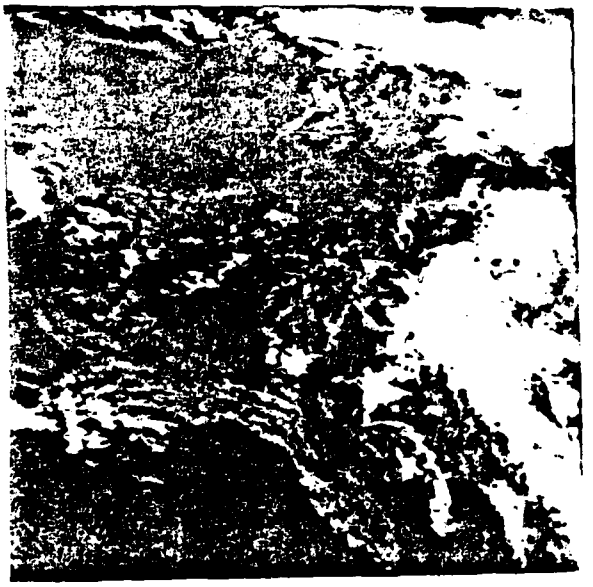

Figure 33. GOES Visible Imagery for 13 May 85

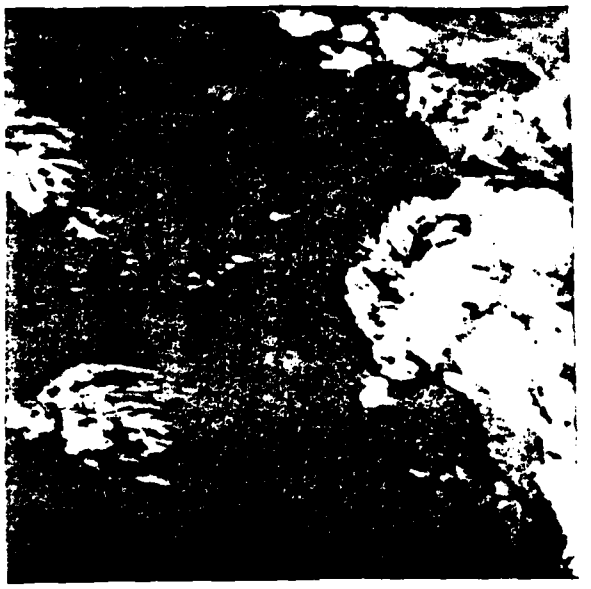

Figure 34. GOES Infrared Imagery for 13 May 85

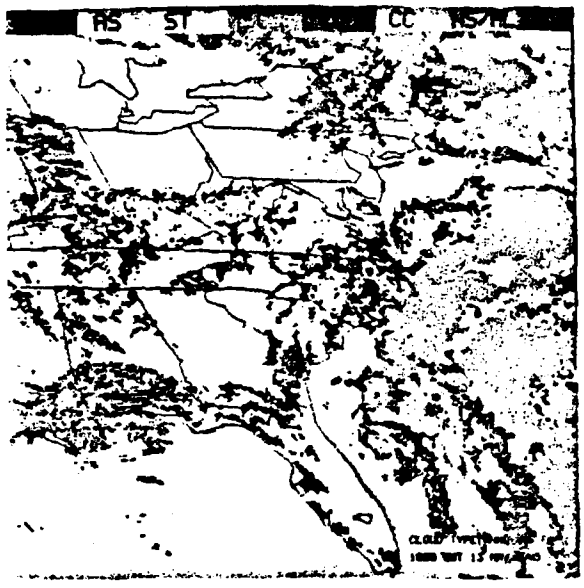

Figure 35. Same as Fig. 16 except for 13 May 85

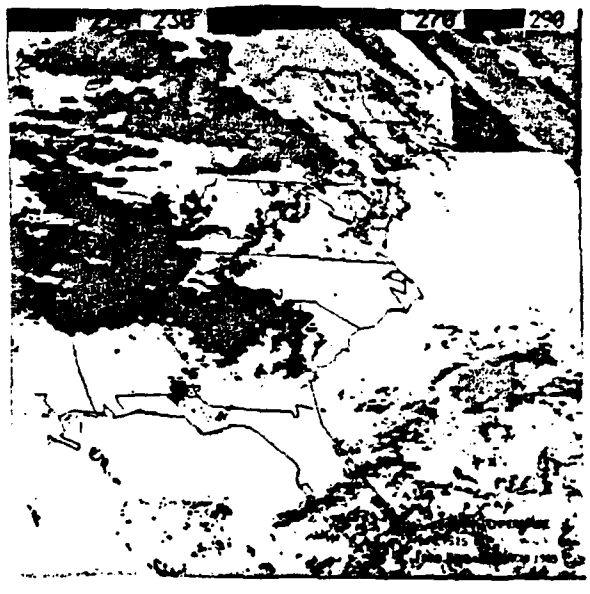

Figure 36. Same as Fig. 17 except for 28 Mar 85

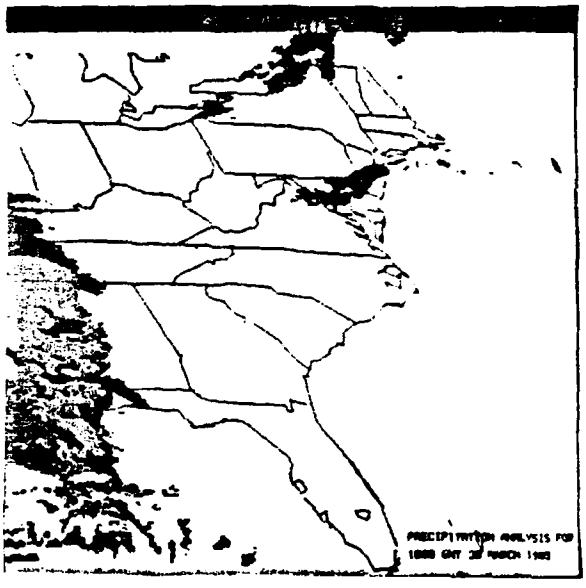

Figure 37. Same as Fig. 20 except for 20 Mar 85

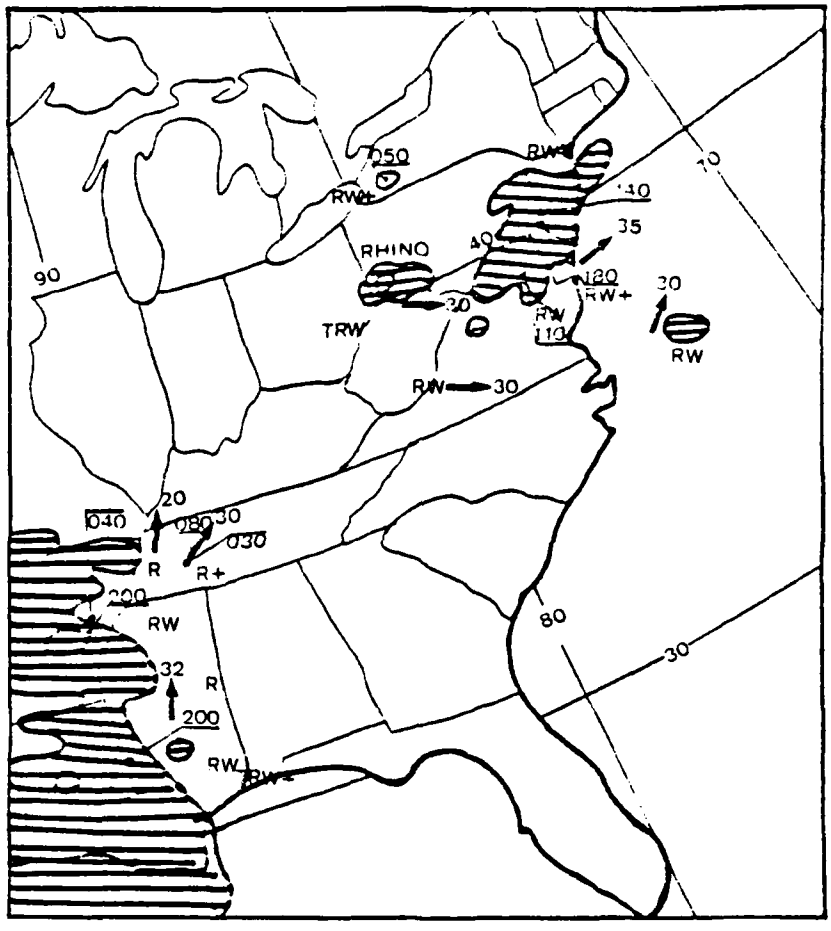

Figure 38. Automated Radar Summary Chart for 20 Mar 85

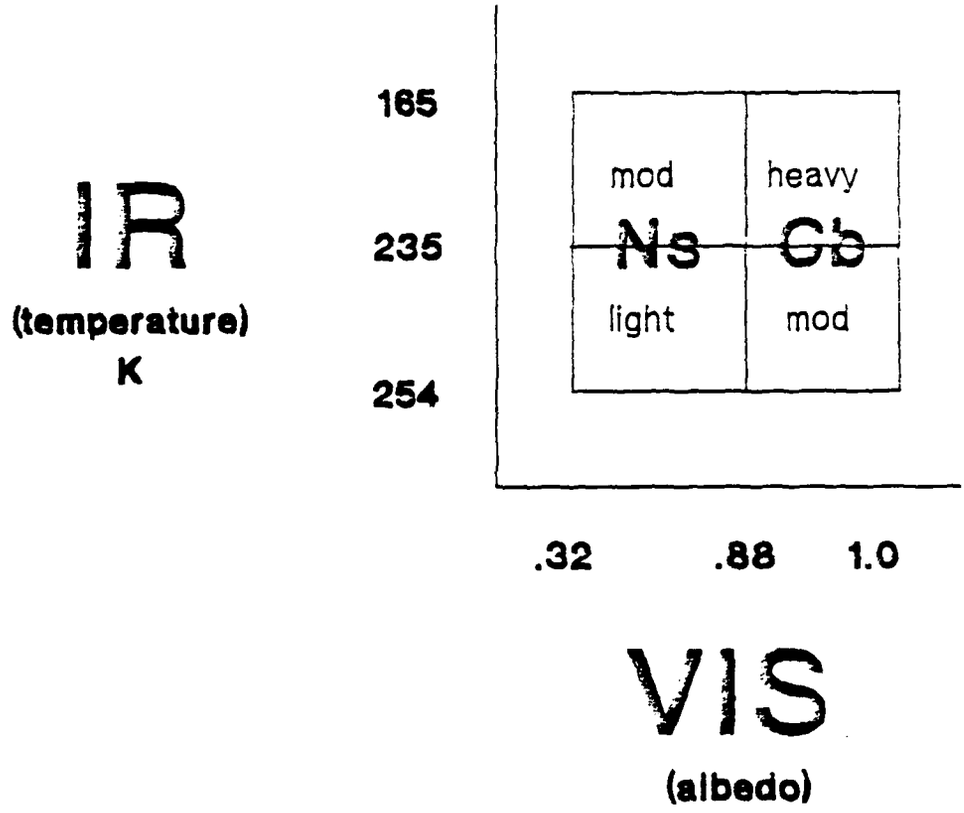

Figure 39. Two-dimensional Precipitation Intensity Estimate Graph Using GOES Infrared and Visible Satellite Digital Data for 20 Mar 85

Figure 40. Same as Fig. 20 except for 11 Apr 85

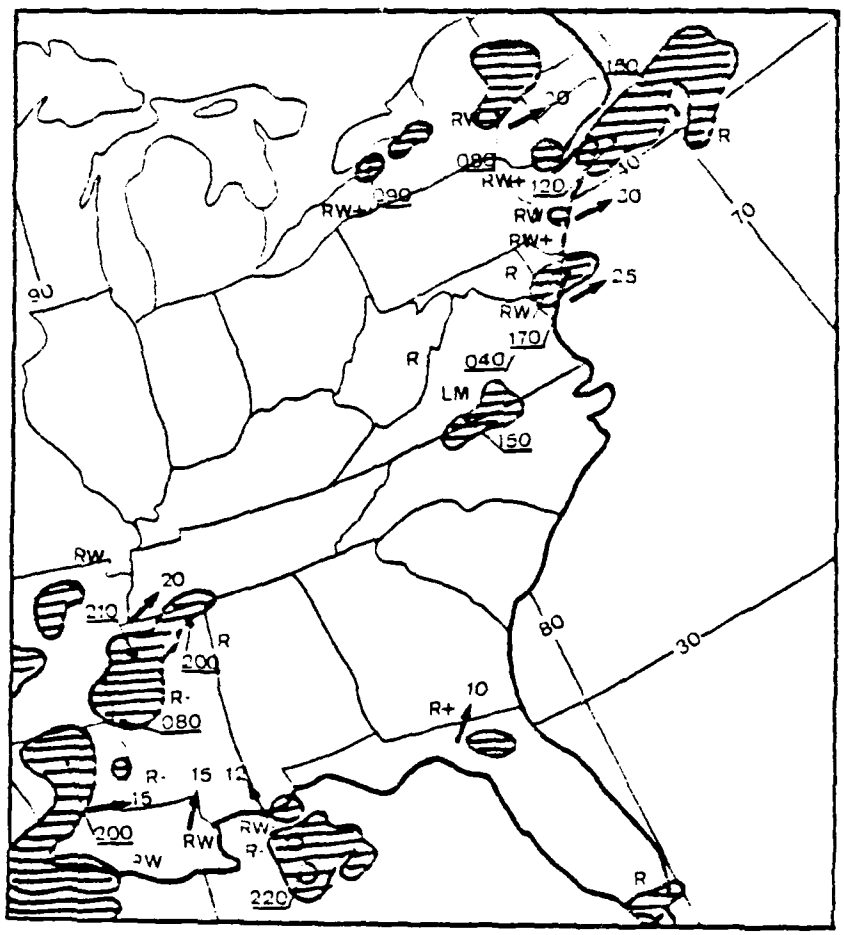

Figure 41. Automated Radar Summary Chart for 11 Apr 85

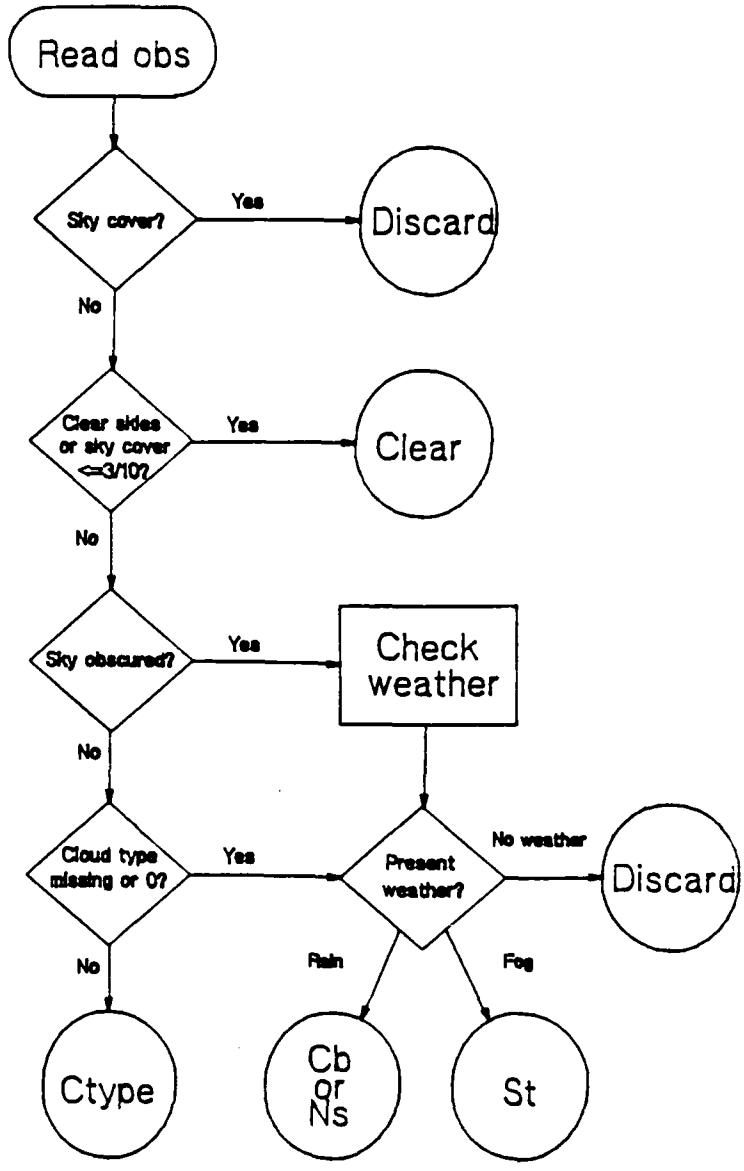

Figure 42. Surface Data Decision Process

AD-A164 441 GEOSTATIONARY SATELLITE ANALYSES OF PRECIPITATION AND CLOUD PARAMETERS(U) NAVAL POSTGRADUATE SCHOOL MONTEREY CA L A SPRAY DEC 85 2/2

UNCLASSIFIED F/G 4/2 NL

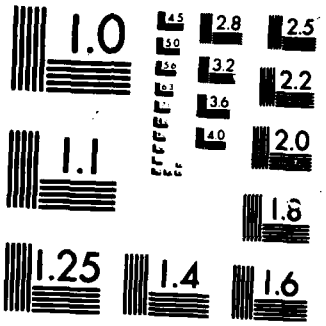

MICROCOPY RESOLUTION TEST CHART
NATIONAL BUREAU OF STANDARDS-1963-A

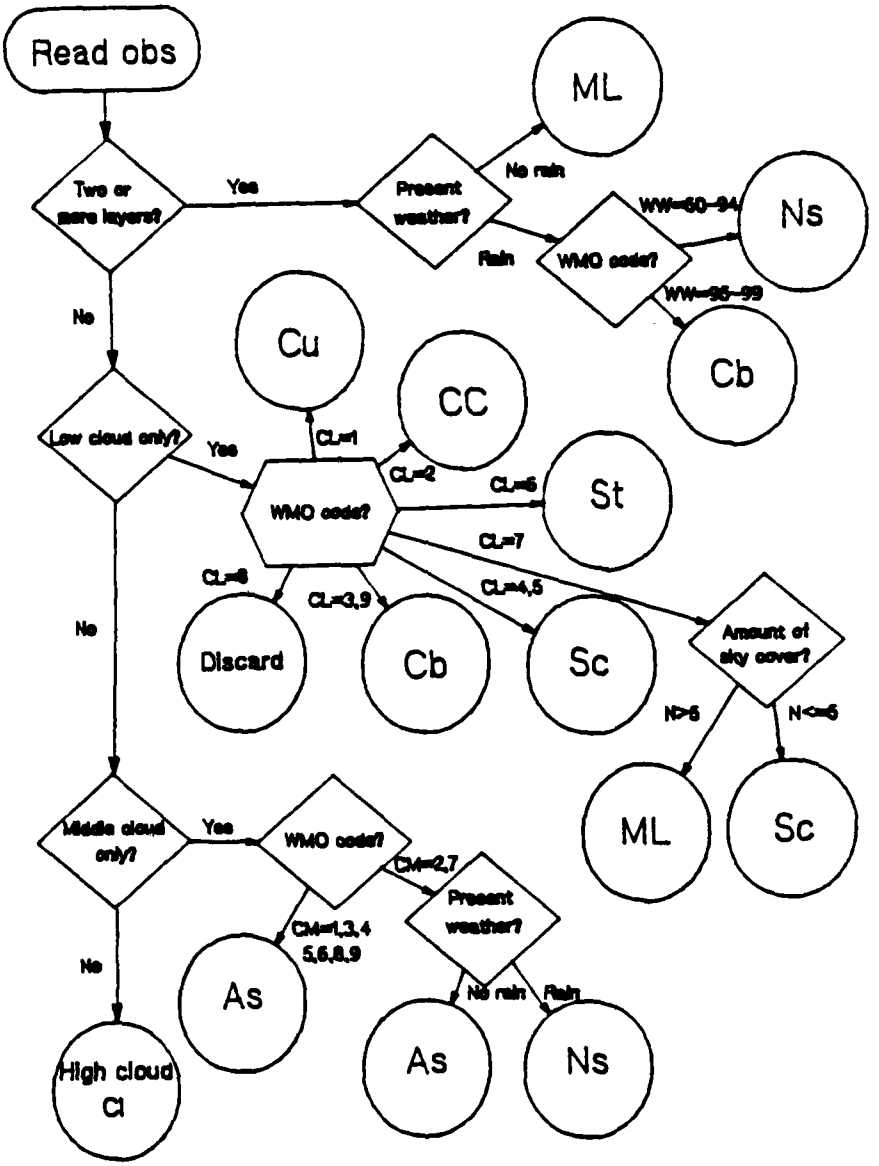

Figure 43. Cloud Type Decision Process

LIST OF REFERENCES

Bunting, J.T. and K.R. Hardy, 1984: Cloud identification and characterization from satellites. Satellite Sensing of a Cloudy Atmosphere , ed. A. Henderson-Sellers, Taylor and Francis, London and Philadelphia, pp. 203-240.

Coakley, J.A., Jr. and D.G. Baldwin, 1984: Towards the objective analysis of clouds from satellite imagery data. J. Appl. Meteor. , 23, pp. 1065-1099.

Corbell, P., C. Callahan and W.J. Kotsch, 1978: The GOES/SMS User's Guide , NOAA National Environmental Satellite Service, (Ref App II Attachment A3).

Fye, F.K., 1978: The AFGWC automated cloud analysis model. AFGWC Technical Memorandum 78-002, H.Q. Air Force Global Weather Central, Offut AFB, Nebraska, 97 pp.

Hahn, C.J., S.G. Warren, J. London, R.M. Chervin, and R. Jenne, 1984: Atlas of simultaneous occurrence of different cloud types over land, NCAR Technical Note, Boulder, CO, 253 pp.

Harris, R. and E.C. Barrett, 1978: Toward an objective neph-analysis. J. Appl. Meteor. , 17, pp. 1258-1266.

Keegan, T.J. and M. Niedzielski, 1981: Specification of cloud amount over local areas from GOES visual imagery. AFGL-TR-81-0153, 61 pp.

Kunde, V.G., 1967: Theoretical computations of the outgoing infrared radiance from a planetary atmosphere. NASA Tn D-4045, Greenbelt, MD, Goddard Space Flight Center, 117 pp.

Liljas, E., 1982: Automated techniques for the analysis of satellite cloud imagery. Nowcasting , ed. K. Browning, Academic Press, London, pp. 177-190.

Liljas, E., 1984: Processed satellite imageries for operational forecasting, Swedish Meteorological and Hydrological Institute, Norrkoping, Sweden, 43 pp.

Lovejoy, S. and G.L. Austin, 1979: The sources of error in rain amount estimating schemes from GOES VIS and IR satellite data. Mon. Wea. Rev. , 107, pp. 1048-1054.

Maturi, E.M. and S.J. Holmes, 1985: Monthly IR imagery enhancement curves: a tool for nighttime sea fog identification off the New England coast. NOAA Technical Memorandum NESDIS12.

Minnis, P. and E.F. Harrison, 1984: Diurnal variability of regional cloud and clear-sky radiative parameters derived from GOES data: part I: analysis method. J. Appl. Meteor. , 23, pp. 993-1011.

Moren, C.A., 1984: An evaluation of the SPADS automated cloud analysis program. M.S. Thesis, Naval Postgraduate School, 137 pp.

Muench, H.S. and T.J. Keegan, 1979: Development of techniques to specify cloudiness and rainfall rate using GOES imagery data. AFGL-TR-79-0255, AD A084, 46 pp.

Paul, L.S., 1983: A study of precipitation occurrence using visual and infrared satellite data. M.S. Thesis, Naval Postgraduate School, 114 pp.

Platt, C.M.R., 1983: On the bispectral method for cloud parameter determination from satellite VISSR data: separating broken cloud and semitransparent cloud. J. Appl. Meteor. , 22, pp. 429-439.

Reynolds, D.W. and T.H. Vonder Haar, 1977: A bispectral method for cloud parameter determination. Mon. Wea. Rev. , 105, pp. 446-457.

Shenk, W.E. and V.V. Salomonson, 1972: A multispectral technique to determine sea surface temperature using Nimbus-2 data. J. Phys. Ocean. , 2, pp. 157-167.

Shenk, W.E., R.J. Holub and R.A. Neff, 1975: A multispectral cloud type identification method developed for tropical ocean areas with Nimbus-3 MRIR measurements. Mon. Wea. Rev. , 104, pp. 284-291.

Tsonis, A.A., 1984: On the separability of various classes from GOES visible and infrared data. J. Appl. Meteor. , 23, pp. 1393-1410.

Wash, C.H., L.A. Spray and L.C. Chou, 1985: Satellite cloud and precipitation analysis using a minicomputer. Technical Report NPS-63-85-003, Naval Postgraduate School, 91 pp.

Wyse, N.R., 1984: The inclusion of surface data into the SPADS cloud analysis model. M.S. Thesis, Naval Postgraduate School, 145 pp.

INITITAL DISTRIBUTION LIST

		No. Copies
1.	Defense Technical Information Center Cameron Station Alexandria, VA 22304-6145	2
2.	Library, Code 0142 Naval Postgraduate School Monterey, CA 93943	2
3.	Professor Robert J. Renard, Code 63Rd Department of Meteorology Naval Postgraduate School Monterey, CA 93943	1
4.	Associate Professor Carlyle H. Wash, Code 63Wx Department of Meteorology Naval Postgraduate School Monterey, CA 93943	12
5.	Assistant Professor Philip A. Durkee, Code 63De Department of Meteorology Naval Postgraduate School Monterey, CA 93943	1
6.	Laura A. Spray 111 Shelter Lagoon Santa Cruz, CA 95060	3
7.	Director Naval Oceanography Division Naval Observatory 34th and Massachusetts Avenue NW Washington, D.C. 20390	1
8.	Commander Naval Oceanography Command NSTL Station Bay St. Louis, MS 39522	1
9.	Commanding Officer Naval Oceanographic Office NSTL Station Bay St. Louis, MS 39522	1

10. Commanding Officer 1
Fleet Numerical Oceanography Center
Monterey, CA 93940

11. Commanding Officer 1
Naval Ocean Research and Development Activity
Monterey, CA 93940

12. Commanding Officer
Naval Environmental Prediction Research Facility 1
Monterey, CA 93940

13. Chairman, Oceanography Department 1
U.S. Naval Academy
Annapolis, MD 21402

14. Chief of Naval Research 1
800 N. Quincy Street
Arlington, VA 22217

15. Office of Naval Research (Code 480) 1
Naval Ocean Research and Development Activity
NSTL Station
Bay St. Louis, MS 39522

END

FILMED

3-86

DTIC